GEOLOGICA CARPATHICA, 2024, 75, 1, 3–20 https://doi.org/10.31577/GeolCarp.2024.02

The petrology and geochronology of the gabbro-dioritoid rocks from Veľké Železné (Nízke Tatry Mts., Western Carpathians)

JÁN SPIŠIAK[1,✉], MILAN KOHÚT[2,✉], JURAJ BUTEK[1], ŠTEFAN FERENC[1], VIERA ŠIMONOVÁ[1], RICHARD KOPÁČIK[1] and DAVID CHEW[3]

[1]Faculty of Natural Sciences, Matej Bel University, Tajovského 40, 974 01 Banská Bystrica, Slovak Republic
[2]Earth Science Institute, Slovak Academy of Sciences, Dúbravská cesta 9, P.O Box 106, 840 05 Bratislava, Slovak Republic
[3]Department of Geology, School of Natural Sciences, Trinity College Dublin, D02PN40 Dublin 2, Ireland

(Manuscript received November 2, 2023; accepted in revised form March 12, 2024; Associate Editor: Igor Broska)

Abstract: The gabbro-dioritoid rocks from Veľké Železné (Nízke Tatry Mts., Western Carpathians, Slovakia) were recently studied in order to better understand the age, origin, and evolution of the basic/intermediate magmas associated with Variscan granitic rocks. Their genesis was investigated from the points of view of petrology, whole-rock geochemistry (including Sr, Nd, and Pb isotopic characteristics), as well as U–Th–Pb zircon and apatite dating. The Famennian magmatic crystallization age of ca. 360 Ma (determined from zircon: 362.4±2.9 Ma and apatite: 358.4±2.8 Ma) is older than the Tournaisian–Visean ages for granite intrusions in the Tatric Unit. Geochemically, the studied rocks have an affinity to arc-related basalts, consisting of a metaluminous, magnesian, and high-potassium calc-alkaline character. Isotope data (i.e., $(^{87}Sr/^{86}Sr)_{360}$=0.7035–0.7044 and εNd_{360}=+1.4 to +1.6) demonstrate that these gabbro-dioritoids were formed from the mantle-influenced, lower crustal and/or sub-continental lithospheric mantle (SCLM) sources, whereas the unsystematic increase of Pb isotope ratios indicate either the melting of an ancient Enriched mantle-II (EM-II) reservoir or the upper crustal assimilation and/or local fluid alteration. The data presented in this paper favour the origin of the studied gabbro-dioritoids at a continental arc, although we cannot rule out their genesis as a result of the subsequent slab break-off.

Keywords: gabbro-dioritoids, petrology, geochemistry, U–Th–Pb zircon & apatite dating, Nízke Tatry Mts., Western Carpathians

Introduction

Gabbro-dioritoids are widespread in orogenic areas worldwide, and if associated with granitic plutons, they provide important clues to their internal compositional variability, rheological history of the magmas, and the mode of pluton emplacement. Gabbro-dioritoids that are coeval with granites can be interpreted in several ways as a product of: (1) fractional crystallization of hornblende, plagioclase, and biotite from the mantle-derived, gabbroic primary melts (Arth et al. 1978; Janoušek et al. 2020); (2) hybridisation of basic (gabbroic/basaltic) and felsic (granitic) magmas (Bowes & McArthur 1976; Pitcher 1997; Bea et al. 1999); (3) partial melting of a lower crustal sources unrelated to those of the granitic host rocks (Arth & Hanson 1972; Jung et al. 2002); (4) syn-plutonic dykes and larger intrusions of basic magma into the unconsolidated and relatively cooler granitic magma (Pitcher 1997). Diorites forming mafic microgranular enclaves (MME) within granites are either explained as: (a) globules of hybrid magmas; (b) restite material, i.e., the solid residue from partial melting of source rocks; (c) xenoliths, i.e., fragments of the country rocks collected during the ascent of the host magma; (d) blobs of quasi-liquid magma derived from comagmatic mafic intrusions (see Didier & Barbarin 1991; Barbarin 2005). Generally, gabbro-dioritoid rocks can shed light on the interactions between two magmas (mixing and mingling processes), as well as the contact relationships between substantial bodies of gabbro and granite, for example, on different sources of rocks or the emplacement levels of intermediate and/or felsic rocks.

In the Central Western Carpathians (CWC), gabbro-dioritoids were described in nearly all of the core mountains of the Tatric Unit as well as in the Veporic composite granitic pluton from a petrologic, geochemical, and geochronological point of view (Kohút et al. 1999; Poller & Todt 2000; Poller et al. 2001, 2005; Gawęda et al. 2005; Uher et al. 2011, 2012; Broska et al. 2022). The Nízke Tatry Mts. (NTM) are one of the best examples of a composite granite body, where gabbro-dioritoids form small bodies and/or MME within granitic host rocks. In the NTM and the neighbouring Vysoké Tatry Mts., an isotopic (Sr, Nd, Pb) characterisation of diorites and their host rocks was made by Poller et al. (2001, 2005). The aim of the current contribution is to present the results of precise in-situ U–Th–Pb zircon and apatite dating together with

✉ corresponding authors: Ján Spišiak jan.spisiak@umb.sk
Milan Kohút milan.kohut@savba.sk

additional radiogenic isotope data from the Veľké Železné locality, as well as discuss the origin of gabbro-dioritoids in both the Nízke Tatry Mts. and the Western Carpathians.

Geological setting

The Nízke Tatry Mountains are situated in the northern sector of Central Slovakia and represent a typical polyorogenic part of the CWC crystalline basement (Fig. 1a, b). Geographically, they form a 90 km long and 25 km wide E–W trending mountain range that is divided into the western, Ďumbier part belonging to the Tatric Unit, and the eastern, Kráľova Hoľa part which is formed by the Veporic Unit. Various types of Variscan granitic rocks were identified within the Ďumbier part of the NTM basement, e.g., medium-grained biotite tonalites to granodiorites (Ďumbier type), coarse-grained porphyritic biotite granodiorites to granites (Prašivá type), and muscovite–biotite leucogranites (Koutek 1931; Lukáčik 1981; Kohút 1998; Broska et al. 2013; Kohút & Larionov 2021; Maraszewska et al. 2022). These magmatic rocks occur together with other crystalline basement rocks such as orthogneisses, paragneisses, migmatites, and amphibolites. The NTM crystalline basement is overlain by the Mesozoic

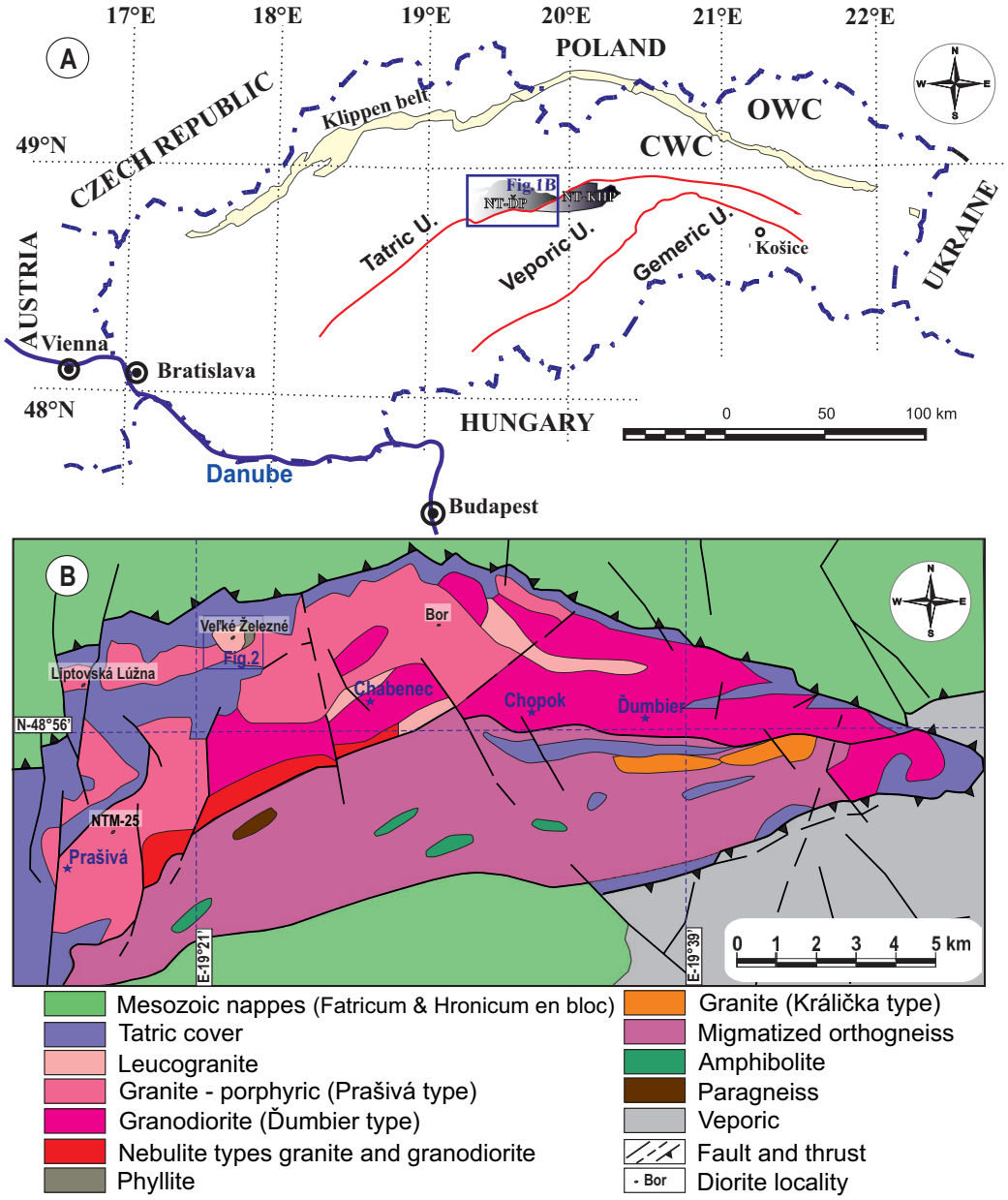

Fig. 1. A — Tectonic scheme of the Western Carpathians (Slovak part), with position of the Nízke Tatry Mountains. *Abbreviations*: CWC – the Central Western Carpathians, OWC – the Outer Western Carpathians, NT-ĎP – Nízke Tatry Mts. Ďumbier part, NT-KHP – Nízke Tatry Mts. Kráľova Hoľa part; **B** — Simplified geological map of the Nízke Tatry Mts. – Ďumbier part according Biely et al. (1992).

Tatric Cover Unit and overthrust by two allochthonous Mesozoic nappes – the Fatric Unit and the Hronic Unit, which occur in a tectonically-higher position (Biely et al. 1992). The crystalline basement, along with its Mesozoic cover and these nappe complexes were juxtaposed by NW-directed thrusting during the Late Cretaceous (Kriváňová et al. 2023). The Ďumbier part of the NTM forms a typical horst structure and was finally exhumed during the Alpine Orogeny in the Eocene period (Danišík et al. 2011).

A characteristic feature of the NTM granitoid pluton is its textural, petrographic, and chemical variability, and for this reason it had been subdivided already by Koutek (1931) into several granitic types (Fig. 1b). The NW part of the NTM comprises the porphyritic Prašivá biotite granite–granodiorite, whereas the NE part is formed by the Ďumbier type biotite tonalite–granodiorite. The Prašivá granite encloses numerous enclaves of Bt- or Amp–Bt quartz diorite, up to tens of cm in diameter, abundant especially in the SW part in the Liptovská Lúžna area (Broska & Petrík 1993; Poller et al. 2005). However, larger (up to tens of meters) bodies of gabbro-dioritoids occur at Bor peak or in the Veľké Železné Valley (Spišiak et al. 2017).

Several occurrences of basic/intermediate igneous rocks are known from the northern slopes of the NTM. Koutek (1931) described one of the dioritoid bodies within the leucocratic granites in the Veľké Železné Valley, which appears about 200 m before the connection with the Malé Železné Valley on the right side of the stream (Fig. 2).

Samples and methods

Samples were taken from different parts of the Veľké Železné body at N 48°58’00.42”, E 19°24’36.42”. For geochemical study, we used samples with the relatively best-preserved primary minerals (the least altered).

Thin sections were studied with a NIKON Eclipse LV 100N microscope. Silicates were studied using the electron microprobe JEOL JXA 8530FE at the Earth Sciences Institute of the Slovak Academy of Sciences in Banská Bystrica under the following conditions: accelerating voltage 15 kV, probe current 20 nA, beam diameter 3–8 µm, ZAF correction, counting time 10 s on peak, 5 s on background. The used standards, X-ray lines and D.L. (in ppm) were: Ca(Kα, 25) – diopside, K (Kα, 44) – orthoclase, P (Kα, 41) – apatite, F (Kα, 167) – fluorite, Na (Kα, 43) – albite, Mg (Kα, 41) – diopside, Al (Kα, 42) – albite, Si (Kα, 63) – quartz, Ba (Lα, 72) – barite, Fe (Kα, 52) – hematite, Cr (Kα, 113) – Cr_2O_3, Mn (Kα, 59) – rhodonite, Ti (Kα, 130) – rutile, Cl (Kα, 12) – tugtupite, Sr (Lα, 71) – celestite.

The whole-rocks chemical compositions were determined at the ACME Analytical Laboratories (now the Bureau Veritas, Vancouver, Canada). Total abundances of major-element oxides were determined by inductively coupled plasma – emission spectrometry (ICP-ES) following lithium metaborate–tetraborate fusion and dilute nitric acid treatment. Loss on ignition (LOI) was calculated from the difference in weight after ignition to 1000 °C. Concentrations of trace elements and rare earth elements were determined by ICP mass spectrometry (ICP-MS). Further details are accessible on the web page of the ACME Analytical Laboratories (http://acmelab.com).

Apatite and zircon separation was conducted by the standard separation procedure of heavy minerals (crushing, sieving, gravitation density separation by using the Wilfley table, heavy liquid – bromoform, electro-magnetic, and hand-picking). All U–Pb data were acquired using a Photon Machines Analyte Exite 193 nm ArF Excimer laser-ablation system with a Helex 2-volume ablation cell, coupled to a Thermo Scientific iCAP Qc at the Department of Geology Trinity College Dublin. 0.65 l/min He carrier gas was split evenly between the large outer sample chamber and the small inner volume (the ‘cup’) where ablation occurs. A small volume of N_2 (ca. 6 ml/min) to enhance signal sensitivity and reduce oxide formation and 0.7 l/min Ar nebulizer gas was then introduced to the sample-gas mixture via an in-house smoothing device. ^{202}Hg, $^{204, 206, 207, 208}$Pb, ^{232}Th and ^{238}U were acquired for all U–Pb analyses. ^{91}Zr and ^{43}Ca were employed as the internal standards for zircon and apatite respectively, while ^{31}P, ^{35}Cl, ^{55}Mn, ^{88}Sr, ^{89}Y and the REE were also acquired for apatite. Analyses employed a 20 µm (zircon) or 60 µm (apatite) laser spot, a 5 Hz laser repetition rate and a fluence of 3.9 J/cm^2.

The raw isotope data were reduced using the “VizualAge” data reduction scheme of Petrus & Kamber (2012) within the freeware IOLITE package of Paton et al. (2011). User-defined time intervals are established for the baseline correction procedure to calculate session-wide baseline-corrected

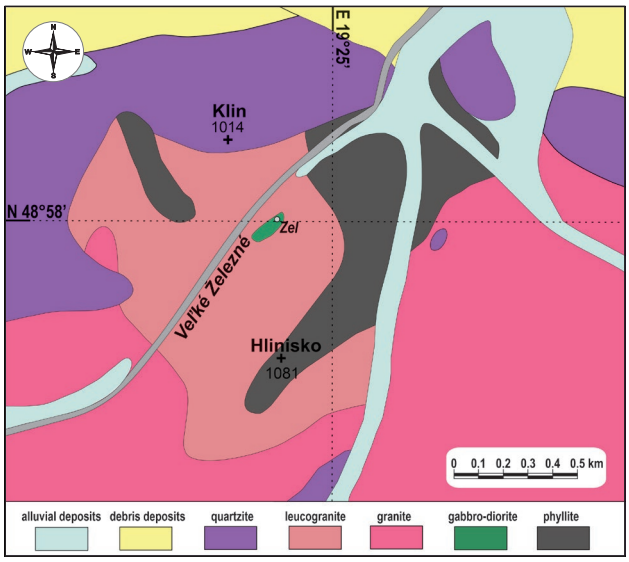

Fig. 2. Geological map of Veľké Železné area. Taken from the Geological map of Slovakia on a scale M 1:50 000 [*online*]. Bratislava: Dionýz Štúr State Institute of Geology, 2013 (http://mapserver.geology.sk/gm50js).

values for each isotope. The time-resolved fractionation response of individual standard analyses is then characterised using a user-specified down-hole correction model (such as an exponential curve, a linear fit, or a smoothed cubic spline). The data reduction scheme then fits this appropriate session-wide "model" U–Th–Pb fractionation curve to the time-resolved standard data and the unknowns. Sample-standard bracketing is applied after the correction of down-hole fractionation to account for long-term drift in isotopic or elemental ratios by normalizing all ratios to those of the U–Pb reference standards. Common Pb in the apatite and rutile standards was corrected using the ^{207}Pb-based correction method using a modified version of the VizualAge DRS, which accounts for the presence of variable common Pb in the primary standard materials (Chew et al. 2014).

For zircon, the analytical procedure employed 91500 zircons (^{206}Pb/^{238}U TIMS age of 1065.4±0.6 Ma; Wiedenbeck et al. 1995) as the primary standard and Temora 2 zircon (^{206}Pb/^{238}U TIMS age of 416.8±1.3 Ma; Black et al. 2003) as the secondary standard. Temora 2 yielded a U–Pb concordia age of 417.2±1.4 Ma (MSWD=0.107; n=33). For apatite, Madagascar apatite (Thomson et al. 2012) (weighted average ID-TIMS concordia age of 473.5±0.7 Ma, Cochrane et al. 2014) was used as the primary apatite reference material. McClure Mountain syenite apatite (weighted mean ^{207}Pb/^{235}U age of 523.51±2.09 Ma, Schoene & Bowring 2006) and Durango apatite (31.44±0.18 Ma, McDowell et al. 2005) were used as a secondary standard. McClure Mountain apatite yielded a weighted average ^{207}Pb-corrected age of 521.2±2.6 Ma (MSWD=1.6; n=56) employing an initial ^{207}Pb/^{206}Pb value of 0.88198 derived from the apatite ID-TIMS total U–Pb isochron (Schoene & Bowring 2006). The Durango apatite standard (McDowell et al. 2005) yielded a weighted average ^{207}Pb-corrected age of 33.1±1.2 Ma (MSWD=1.5; n=16) employing an initial ^{207}Pb/^{206}Pb value derived from the terrestrial crustal evolution model by Stacey & Kramers (1975).

The Sr–Nd–Pb isotopic analyses were carried out using a VG Sector 54 IT Thermal Ionization Mass Spectrometer (TIMS) at the Danish Centre for Isotope Geology, University of Copenhagen. For the radiogenic isotope analyses, the powdered samples were dissolved by standard procedures using concentrated HNO_3, HCl, and HF within Savillex™ beakers on a hotplate at 130 ºC for 3 days. A ^{150}Nd/^{147}Sm spike was added beforehand. The isotopic ratios of Sm, Nd, Pb, and Sr, as well as of Sm and Nd isotopic dilution concentrations, were determined from separately-dissolved powder aliquots. Samples were separated over chromatographic columns charged with a 12 ml AG50W-X 8 (100–200 mesh) cation resin, whereby Sr and REE fractions were collected. The REE fractions were further separated over smaller chromatographic columns containing Eichrom's™ LN resin SPS (Part#LN-B25-S). Strontium cuts were purified by applying a standardized 3M HNO_3–H_2O elution recipe on self-made disposable mini-extraction columns, which consisted of 1ml pipette tips in which we fitted a frit filter to retain a 0.2 ml intensively pre-cleaned mesh 50–100 Sr Spec™ (Eichrom Inc.) resin. The elution recipe essentially followed that of Horwitz et al. (1992) and was scaled to our needs. Strontium was eluted/stripped by pure deionised water, and the eluate was dried afterwards on a hotplate.

Samarium isotopes were measured in a static multi-collection mode, whereas Nd isotopes were collected in a multi-dynamic routine, both on a triple Ta–Re–Ta filament assembly. The measured Nd isotope ratios were normalized to ^{146}Nd/^{144}Nd =0.7219. Our measurements of the JNdi-1 standard (Tanaka et al. 2000; 0.512115±7) yielded a mean ^{143}Nd/^{144}Nd value of 0.512105±5 (2σ; n=8) during the period when the samples were analysed. Precision for ^{147}Sm/^{144}Nd ratios is better than 2 % (2σ). Chemical separation of Pb from the whole rock samples was performed over a conventional glass stem and subsequently with miniature glass stem anion exchange columns containing 1 ml and 200 µl of 100–200 mesh Bio-Rad AG 1×8 resin respectively. Lead was analysed in a static multi-collection-mode, whereby the fractionation was controlled by repeated analysis of the NBS 981 standard using the values of Todt et al. (1993). The average fractionation amounted to 0.105±0.008 % (2σ, n=5) per atomic mass unit. Total procedural blanks remained below <200 pg Pb, which were compared to >100 ng Pb loads, though they insignificantly affected the measured Pb isotopic ratios of the samples.

Results

Petrology

There are two rock types at the outcrop. The body consists mainly of a medium-grained rock, phaneritic texture with porphyric biotites (Fig. 3). The marginal parts are formed by a finer-grained variety. However, these parts are more altered than the central part of the body. Macroscopically, the studied gabbro-dioritoid is dark-grey/green in colour and has an equigranular and porphyritic texture (Fig. 3a, b). The groundmass is fine- to medium-grained and moderately altered. The phenocrysts are mainly of black biotite (Fig. 3b). Both biotite phenocrysts and small flakes in the groundmass show strong pleochroism and often resorbed rims (Fig. 4a, b). Pleochroic haloes with locally-preserved zircons are common (Fig. 4e, Table 1). However, primary biotite-I is almost completely replaced by secondary biotite-II and has been preserved only as relics (Fig. 5b, anal. N. 22, 23). Based on the classification of Rieder et al. (1998), all analyses correspond to annite, albeit close to the boundary of the phlogopite field (Fig. 6). The chemical compositions of the two generations of biotite are similar (Table 1).

Amphiboles form phenocrysts or small, often euhedral crystals in the groundmass. They probably coexisted with biotite-I; locally, we observe amphibole inclusions in biotite-II or the biotization of amphiboles. Amphiboles are altered (Figs. 4c, d, and 5a, b) and partly chloritized (Fig. 7b), and the product of their alteration is also small carbonates (Fig. 7b). Based on the IMA classification (Fig. 8, Table 2; Hawthorne et al. 2012),

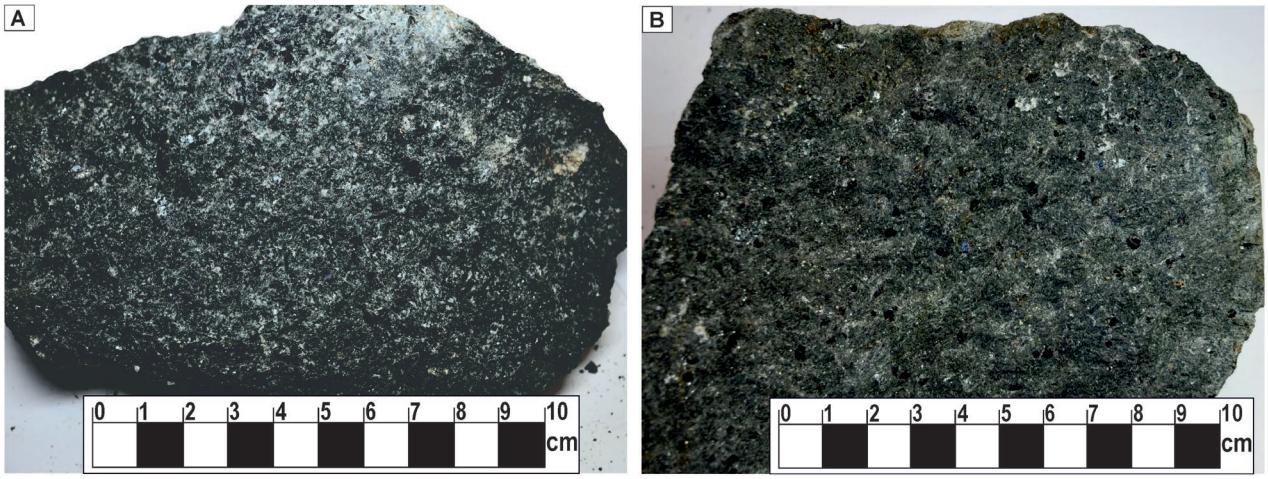

Fig. 3. Macro photographs of gabbro-dioritoids from Veľké Železné: **A** — marginal parts of body with fine- to medium-grained texture (Zel-1b); **B** — phaneritic texture with porphyric biotite (Zel-1c).

the studied amphiboles correspond to magnesio-hornblende, with some points shifted towards the tremolite field.

Plagioclase and quartz are the most common felsic minerals, whereas potassium feldspar is subordinate. Plagioclase is locally altered. Primary plagioclase-I with [$An_{(\geq 50)}$] was saussuritized (Figs. 5, 9) as indicated by the presence of small calcite grains (Figs. 5a, 9b). Plagioclase-II $An_{(25-31)}$ (Table 3, Figs. 9, 10) is locally replaced by albite (Fig. 10b). Albite often forms rims around potassium feldspars as well (Fig. 10c). Potassium feldspars are also locally altered (Fig. 10a) and are Ab-poor (Table 3). Quartz commonly shows strong undulose extinction. Accessory minerals include apatite (hexagonal and short prismatic cross-sections – Fig. 4f) and zircon (Fig. 4e). Pyrite, hematite and goethite are present as opaque minerals.

Whole-rocks major- and trace-element geochemistry

The bulk chemical composition of the gabbro-dioritoids is relatively homogeneous within the Veľké Železné body (Table 4). For better understanding of their character, we have compared their composition with published data for the NTM dioritoids (e.g., Kohút & Recio 2002; Poller et al. 2005; Magna et al. 2010; Maraszewska et al. 2022). It is obvious that the Veľké Železné gabbro-dioritoids represent the most primitive variety among the basic–intermediate rocks associated with granitic rocks in the NTM (Table 4).

Since the studied rocks are partly altered, the Zr/Ti vs. Nb/Y diagram (Pearce 1996; Fig. 11) was chosen for their classification. However, notable differences in the contents of the major- and some trace-elements do not appear in this plot, and the studied gabbro-dioritoids display affinity to basalts, whereas other dioritic rocks from the NTM indicate a rather basaltic andesite character. Moreover, increased K_2O content points to affiliation to the high-potassium calc-alkaline series (Fig. 12a). Predominantly low A/CNK values (Shand 1943) (Table 4) generally show a metaluminous character of the NTM gabbro-dioritoids (Fig. 12b). Increased values of MgO and lower values of Fe-number ($FeO^{tot}/(FeO^{tot}+MgO)$ document their magnesian character (Table 4). Interestingly, the composition of the Veľké Železné samples in the multicationic diagram P–Q (Debon & Le Fort 1983) corresponds to quartz monzonite, whereas the other NTM dioritic rocks are classified as quartz monzodiorites to granodiorites (Fig. 12c).

Trace-element patterns normalized to the Primitive mantle (Sun & McDonough 1989) show significant enrichment in the large-ion lithophile elements (LILE), such as Cs, Rb, Ba, K, Pb. In contrast, they are partly depleted in the high-field-strength elements (HFSE) like Nb, Ta, Zr, Ti (Fig. 13a). The C1 chondrite normalized REE pattern (Boynton 1984) has a relatively steep course with significant LREE enrichment and HREE depletion (La_N/Yb_N=13.1–15.5), having a very small Eu anomaly (Eu/Eu*=0.83–0.86), see Fig. 13b.

Zircon and apatite U–Th–Pb dating

A total of 31 zircon grains were separated from the Veľké Železné gabbro-dioritoid sample Zel-1, of which 18 were suitable for measurement by LA-ICP-MS, and only 10 of the obtained zircon U–Th–Pb analyses provided reasonable results. In contrast, 39 of the total 40 apatite grains in the epoxy mount were successfully analysed. LA-ICP-MS U–Th–Pb isotopic data are listed in the Supplementary Tables S1 (zircons) and S2 (apatites).

Zircon U–Th–Pb analyses are presented on the Wetherill Concordia diagram (Fig. 14a), whereas apatite data are interpreted by the Tera-Wasserburg plot (Fig. 14b). The obtained ages of 362.4±2.9 Ma (zircon concordia age) and 358.4±2.8 Ma (apatite; lower intercept age) overlap within the error. They indicate a Famennian (ca. 360 Ma) emplacement and fast

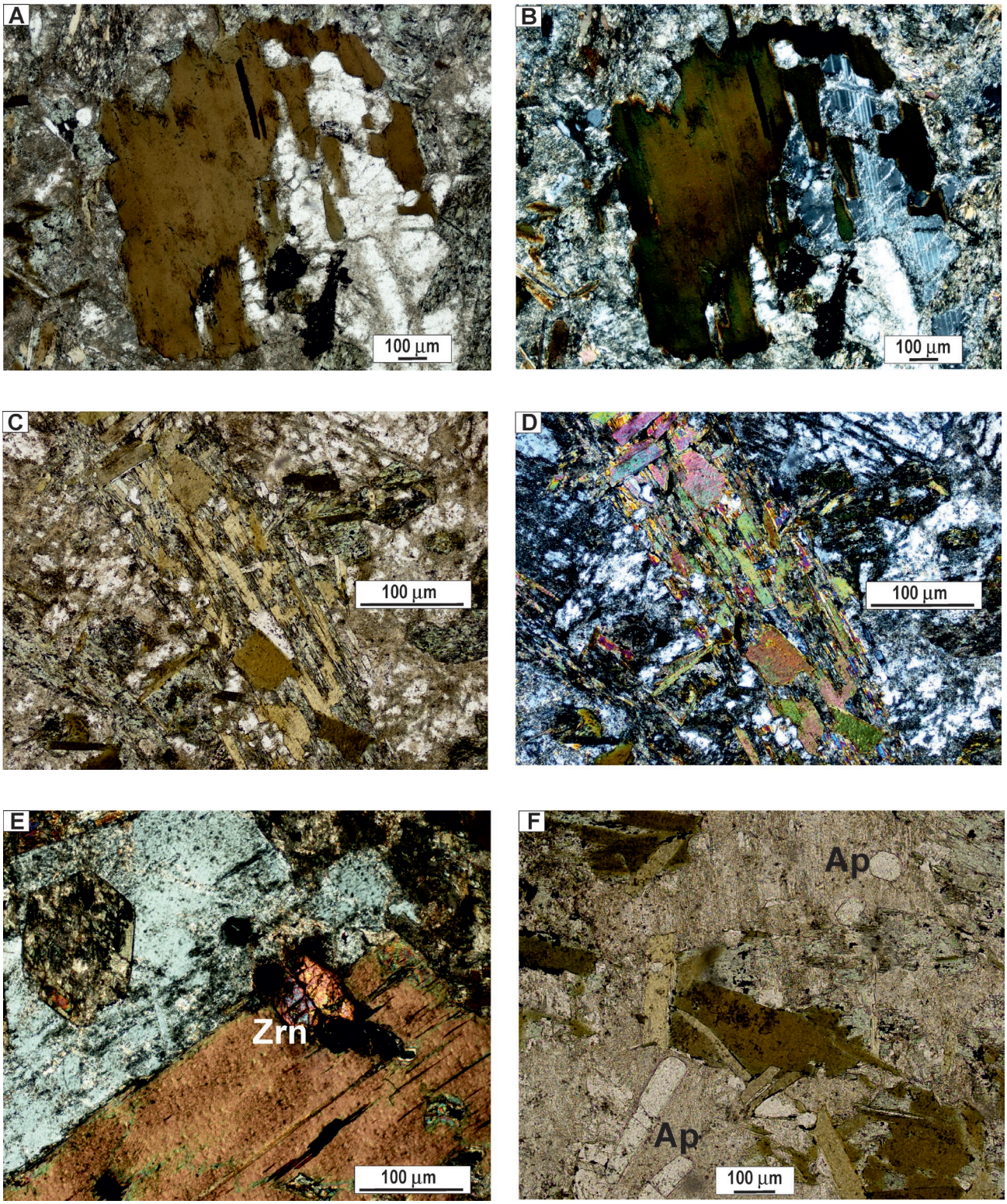

Fig. 4. Photomicrographs of gabbro-dioritoid from Veľké Železné, sample Zel-1c: **A** — biotite phenocryst, plane polarized light; **B** — the same, crossed nicols; **C** — altered amphiboles, plane polarized light; **D** — the same, crossed nicols; **E** — zircon in biotite crossed nicols; **F** — columnar and basal section apatite, plane polarized light. *Abbreviations*: Zrn – zircon, Ap – apatite**.**

Table 1: The chemical composition of the studied biotites.

N. anal.	Bt-4	Bt-1	Bt-8	1	3	4	9	10	11	12	13	14	15	16	17	20	22	23
Fig.	Fig-6a	Fig-8a	Fig-8b	Fig-4a	Fig-4a	Fig-4a	Fig-4a	Fig-4a	Fig-4a	Fig-4a	Fig-4a	Fig-4b	Fig-4b	Fig-4b	Fig-4b	Fig-4b	Fig-4b	Fig-4b
SiO_2	37.62	38.72	38.72	37.92	37.87	37.51	37.89	37.59	37.77	38.09	37.53	37.75	37.59	37.78	37.59	37.68	41.23	41.43
TiO_2	3.84	3.05	2.82	3.48	4.34	3.60	3.58	3.94	4.02	3.64	3.74	3.95	4.68	3.71	3.72	3.48	3.30	3.31
Al_2O_3	14.38	14.49	14.98	14.96	14.75	15.42	14.99	15.12	15.32	15.52	14.94	15.35	14.86	14.99	15.07	15.42	12.06	11.67
Cr_2O_3	0.08	0.00	0.00	0.08	0.20	0.13	0.05	0.04	0.11	0.11	0.07	0.07	0.03	0.11	0.02	0.06	0.02	0.05
FeO*	15.22	14.72	14.11	14.55	14.37	13.90	14.55	14.49	14.62	14.53	14.40	14.35	14.61	14.84	14.94	14.50	12.48	11.94
MnO	0.18	0.19	0.17	0.13	0.14	0.18	0.14	0.18	0.19	0.21	0.16	0.14	0.23	0.21	0.21	0.21	0.16	0.08
CaO	0.02	0.00	0.00	0.00	0.05	0.01	0.01	0.07	0.06	0.01	0.01	0.01	0.01	0.01	0.02	0.01	0.01	0.17
MgO	14.06	13.94	14.92	14.06	14.47	14.35	14.20	13.99	14.08	14.13	14.12	13.92	13.70	13.89	13.70	13.66	16.31	17.03
Na_2O	0.16	0.11	0.13	0.23	0.12	0.11	0.16	0.15	0.14	0.12	0.07	0.13	0.14	0.13	0.09	0.16	0.05	0.07
K_2O	9.57	10.03	10.12	9.54	9.55	9.66	9.58	9.60	9.68	9.72	9.60	9.83	9.74	9.74	9.66	9.76	9.50	9.50
Cl	0.08	0.06	0.04	0.06	0.04	0.04	0.04	0.04	0.03	0.04	0.04	0.04	0.05	0.04	0.04	0.05	0.03	0.03
F	0.00	0.00	0.00	0.00	0.00	0.00	0.00	0.00	0.00	0.00	0.33	0.00	0.25	0.00	0.31	0.00	0.00	0.00
Total	95.20	95.30	96.01	95.02	95.89	94.89	95.19	95.22	96.01	96.12	95.03	95.55	95.88	95.44	95.36	94.99	95.14	95.28
Formula based on 24 oxygens																		
Si	5.643	5.780	5.719	5.669	5.609	5.603	5.653	5.611	5.594	5.626	5.631	5.614	5.599	5.639	5.633	5.640	6.056	6.065
Ti	0.434	0.342	0.314	0.391	0.483	0.405	0.402	0.442	0.448	0.405	0.422	0.442	0.524	0.416	0.419	0.392	0.365	0.364
Al	2.543	2.549	2.609	2.637	2.574	2.714	2.636	2.661	2.674	2.702	2.643	2.690	2.609	2.636	2.662	2.720	2.088	2.014
Al^{IV}	2.357	2.220	2.281	2.331	2.391	2.397	2.347	2.389	2.406	2.374	2.369	2.386	2.401	2.361	2.367	2.360	1.944	1.935
Al^{VI}	0.186	0.328	0.328	0.305	0.183	0.317	0.289	0.273	0.268	0.328	0.274	0.304	0.207	0.275	0.295	0.360	0.144	0.079
Fe"	1.909	1.837	1.743	1.819	1.780	1.736	1.815	1.809	1.811	1.794	1.806	1.785	1.820	1.853	1.873	1.816	1.533	1.462
Mn	0.022	0.024	0.021	0.016	0.017	0.023	0.017	0.023	0.023	0.026	0.021	0.018	0.029	0.027	0.026	0.026	0.020	0.010
Mg	3.144	3.102	3.286	3.133	3.195	3.194	3.158	3.114	3.109	3.112	3.159	3.086	3.042	3.089	3.061	3.048	3.571	3.716
Ca	0.003	0.000	0.000	0.000	0.007	0.001	0.001	0.011	0.010	0.002	0.002	0.001	0.002	0.002	0.002	0.001	0.002	0.026
Na	0.045	0.030	0.037	0.066	0.036	0.031	0.047	0.045	0.041	0.036	0.021	0.036	0.039	0.038	0.027	0.047	0.014	0.020
K	1.831	1.909	1.906	1.819	1.804	1.840	1.823	1.828	1.829	1.830	1.837	1.864	1.850	1.854	1.847	1.864	1.779	1.774
F	0.000	0.000	0.000	0.000	0.000	0.000	0.000	0.000	0.000	0.000	0.158	0.000	0.117	0.000	0.147	0.000	0.000	0.000
Cl	0.020	0.014	0.010	0.015	0.010	0.009	0.011	0.011	0.008	0.010	0.011	0.011	0.012	0.010	0.010	0.012	0.006	0.008
SUM	18.140	18.137	18.254	18.203	18.089	18.271	18.199	18.216	18.220	18.244	18.354	18.238	18.250	18.201	18.370	18.286	17.522	17.473
Fe/Fe+Mg	0.378	0.372	0.347	0.367	0.358	0.352	0.365	0.367	0.368	0.366	0.364	0.366	0.374	0.375	0.380	0.373	0.300	0.282

FeO* is total Fe as FeO

magmatic crystallization due to rapid cooling of the studied gabbro-dioritoids.

Isotope composition

Rb–Sr and Sm–Nd isotopes

The Rb–Sr and Sm–Nd isotopic data of the studied gabbro-dioritoids, along with the isotopic composition of other dioritic rocks from the NTM (Poller et al. 2005), are listed in Table 5, and the $\varepsilon Nd_{(360)}$ vs. $^{87}Sr/^{86}Sr_{(360)}$ plot is presented in Fig. 15. The initial strontium $(^{87}Sr/^{86}Sr)_{360}$ ratios in the NTM diorites are low (0.7035–0.7048). Moderate initial neodymium $[(^{143}Nd/^{144}Nd)_{360}=0.51223–0.51226]$ ratios translate to slightly-positive epsilon Nd values $[\varepsilon Nd_{(360)}=+1.22$ to $+1.60]$. Depleted-mantle Nd model ages (t_{DM2st} ages) for the NTM dioritoids range from 0.94 to 0.97 Ga (Table 5).

Lead isotopes

The Pb isotopic ratios from the studied gabbro-dioritoid sample Zel-2 are listed in Table 6, and the $^{207}Pb/^{204}Pb$ vs. $^{206}Pb/^{204}Pb$ plot is presented in Fig. 16. Lead isotopic composition with present-day $^{206}Pb/^{204}Pb=19.347$, $^{207}Pb/^{204}Pb=15.657$, and $^{208}Pb/^{204}Pb=38.986$ is mildly radiogenic relative to other CWC Variscan intrusive rocks, and plot above the Pb evolution curve of Stacey & Kramers (1975), indicating that its source likely underwent a pre-Variscan increase in U/Pb and Th/U. Lead isotopic ratios of this sample are slightly elevated compared to diorites worldwide, and its projection point falls between the North Hemisphere Reference Line (NHRL) and 4.55 Ga Geochron (White 2013), which indicates an enrichment of the original mantle/lower crustal source by crustal EM-II material (Fig. 16).

Discussion

Geochemistry – tectonic implications

Geochemical fingerprinting is a conventional tool for understanding the magmatic provinces in a tectonic context, and its relation to the igneous rock's genesis (e.g., Pearce & Cann 1973; Wood 1980; Pearce et al. 1981; Meschede 1986; Cabanis

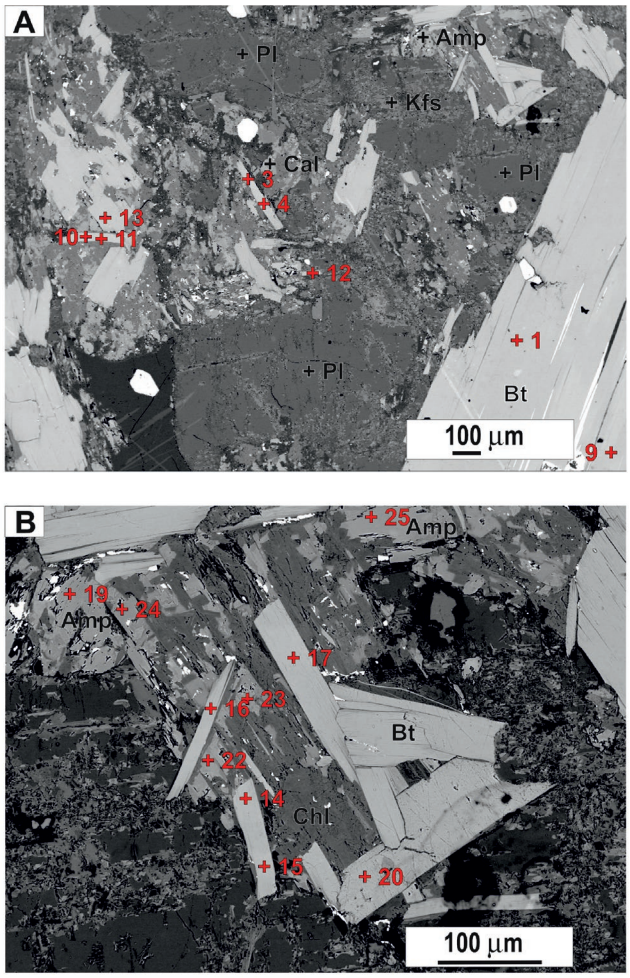

Fig. 5. Back scattered electron (BSE) images of biotites in studied gabbro-dioritoids (Zel-1c); the numbers in figures correspond to those in Tables 1, 2. *Abbreviations*: Pl – plagioclase, Amp – amphibole, Bt – biotite, Chl – chlorite, Cal – calcite.

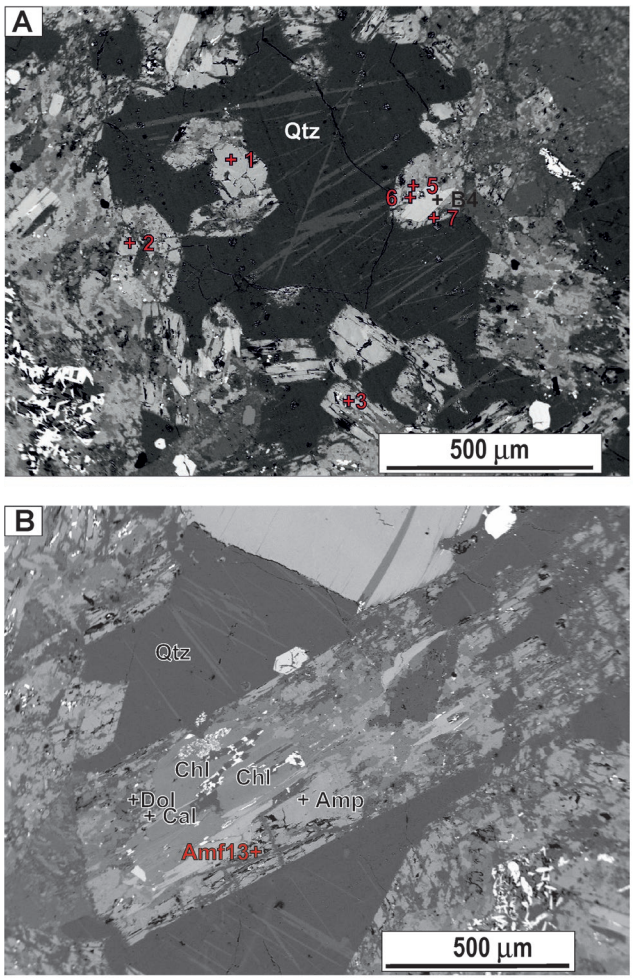

Fig. 7. Back scattered electron (BSE) images of amphiboles in studied gabbro-dioritoids (Zel-1c); the numbers in figures correspond to those in Table 2. *Abbreviations*: Pl – plagioclases, Bt – biotite, Chl – chlorite, Cal – calcite, Dol – dolomite, Qtz – quartz.

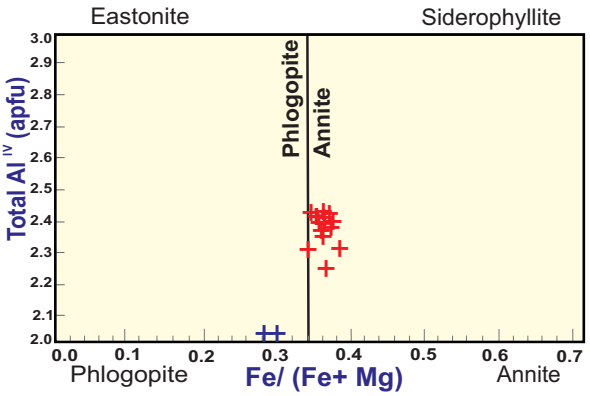

Fig. 6. Classification diagram of studied micas. End-members names according to Rieder et al. (1998).

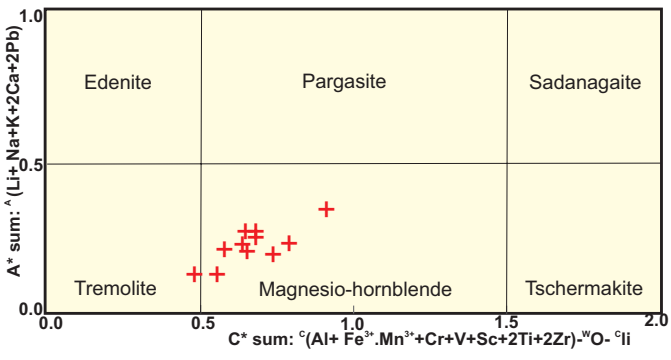

Fig. 8. Classification diagram of amphiboles (Hawthorne et al. 2012).

Table 2: The chemical composition of the studied amphiboles.

N. anal.	1	2	3	5	6	7	Amf13	19	24	25
Fig.	Fig. 6a	Fig. 6a	Fig. 6a	Fig. 6a	Fig. 6a	Fig. 6a	Fig. 6b	Fig. 4b	Fig. 4b	Fig. 4b
SiO_2	48.78	49.42	49.03	46.35	49.10	48.80	50.36	51.25	51.29	49.21
TiO_2	0.77	0.80	0.81	1.18	0.95	0.78	0.55	0.46	0.47	0.84
Al_2O_3	6.40	5.77	6.18	8.23	6.94	5.94	5.09	4.89	4.95	6.43
Cr_2O_3	0.05	0.02	0.04	0.06	0.05	0.09	0.04	0.03	0.00	0.03
FeO*	11.34	10.94	11.21	12.66	11.59	11.32	10.33	10.06	10.06	10.70
MnO	0.25	0.25	0.23	0.25	0.29	0.28	0.26	0.27	0.24	0.29
CaO	12.14	12.07	12.02	11.97	11.91	12.10	11.98	12.11	12.31	12.03
MgO	15.27	15.77	15.60	14.12	15.38	15.43	16.58	16.16	15.82	14.98
NiO	0.00	0.00	0.00	0.00	0.01	0.01	0.00	0.00	0.00	0.00
Na_2O	0.84	0.79	0.72	1.02	0.89	0.90	0.78	0.67	0.59	0.84
K_2O	0.41	0.38	0.37	0.62	0.44	0.38	0.42	0.18	0.13	0.28
Cl	0.04	0.03	0.03	0.06	0.05	0.04	0.03	0.02	0.01	0.03
Total	96.31	96.22	96.24	96.52	97.58	96.07	96.43	96.12	95.89	95.66
Formula based on 23 anions										
Si	7.12	7.19	7.13	6.81	7.07	7.14	7.28	7.40	7.45	7.21
Al^{IV}	0.88	0.81	0.87	1.19	0.94	0.86	0.72	0.60	0.55	0.79
Al^{VI}	0.22	0.18	0.19	0.24	0.24	0.17	0.15	0.29	0.30	0.32
Ti	0.09	0.09	0.09	0.13	0.10	0.09	0.06	0.07	0.05	0.09
Fe^{3+}	0.28	0.28	0.36	0.40	0.33	0.30	0.30	0.12	0.09	0.13
Fe^{2+}	1.10	1.05	1.01	1.16	1.06	1.09	0.95	1.19	1.14	1.18
Mn	0.03	0.03	0.03	0.03	0.04	0.03	0.03	0.03	0.00	0.04
Ca	1.90	1.88	1.87	1.89	1.84	1.90	1.86	1.88	1.92	1.89
Mg	3.32	3.42	3.38	3.09	3.30	3.37	3.57	3.33	3.43	3.27
Na	0.18	0.16	0.14	0.23	0.16	0.20	0.14	0.10	0.17	0.24
K	0.08	0.07	0.07	0.12	0.08	0.07	0.08	0.04	0.03	0.05
Cl	0.01	0.01	0.01	0.01	0.01	0.01	0.01	0.01	0.00	0.01
SUM	15.26	15.23	15.20	15.34	15.24	15.27	15.22	15.14	15.13	15.22

FeO* is total Fe as FeO

& Lecolle 1989; Hollocher et al. 2012; Saccani 2015). Using these classic diagrams (e.g., Pearce & Cann 1973; Wood 1980; Pearce et al. 1981; Hollocher et al. 2012; Saccani 2015 – see Fig. 12d as an example), the studied gabbro-dioritoids correspond to the continental arc-related basalts (CAB). Typical of such arc-related basalts is mantle enrichment via a slab-derived fluid/melt phase, with or without the mixing of melts from various sources (Wang et al. 2016). This genesis is supported by the contents of trace elements in the studied gabbro-dioritoids with typical enrichment in the LILE and depletion in the HFSE (Fig. 14), due to the crust–mantle interaction in the subduction zone (Pearce et al. 1981; Wang et al. 2016). For instance, elevated Th/Yb (4.1–7.7) and moderate Ta/Yb (0.28–0.31) indicate subduction enrichment and origin at a continental magmatic arc (Pearce et al. 1981).

Age

Since the age of these rocks was unknown, various authors (e.g., Koutek 1931; Hovorka 1967 and others) considered the gabbro-dioritoids from Veľké Železné to be equivalent to the Permian lamprophyres known from the southern slopes of the Nízke Tatry Mts. or from the Malá Fatra Mts. Our new U–(Th)–Pb dating using the LA-ICP-MS sheds new light on the genesis of the dioritic rocks in the Western Carpathians. The ~360 Ma magmatic age of the Veľké Železné Valley gabbro-dioritoids (zircon: 362.4±2.9 Ma; and apatite: 358.4±2.8 Ma) is significantly higher than the first modern isotopic single-grain TIMS zircon U–Th–Pb age from the Vysoké Tatry Mts. of 341±5 Ma (Poller & Todt 2000). Interestingly, a Visean age (of ca. 340±4 Ma) provided a more recent apatite U–Pb dating (Gawęda et al. 2014) of the Vysoké Tatry Mts. diorites. Lastly, a comparable young age of 341.6±2.4 Ma was obtained for diorite from the Modra Massif (Malé Karpaty Mts.) by U–Pb SHRIMP zircon dating (Uher et al. 2011). Curiously, diorite from the Bratislava Massif (also Malé Karpaty Mts.) gave an older magmatic age of 353±2.3 Ma (Uher et al. 2011) as did diorite from Bor (Nízke Tatry Mts.; 350±2.4 Ma: Uher et al. 2011).

Recently, Broska et al. (2022) published U–Pb SHRIMP zircon age of 359.2±3.0 Ma for diorite from the same locality as Poller & Todt (2000). In any case, subsequent massive intrusions of the granitic rocks in the Western Carpathians culminated within the 353–350 Ma time interval (Kohút et al. 2009; Broska et al. 2013, 2022; Kohút & Larionov 2021).

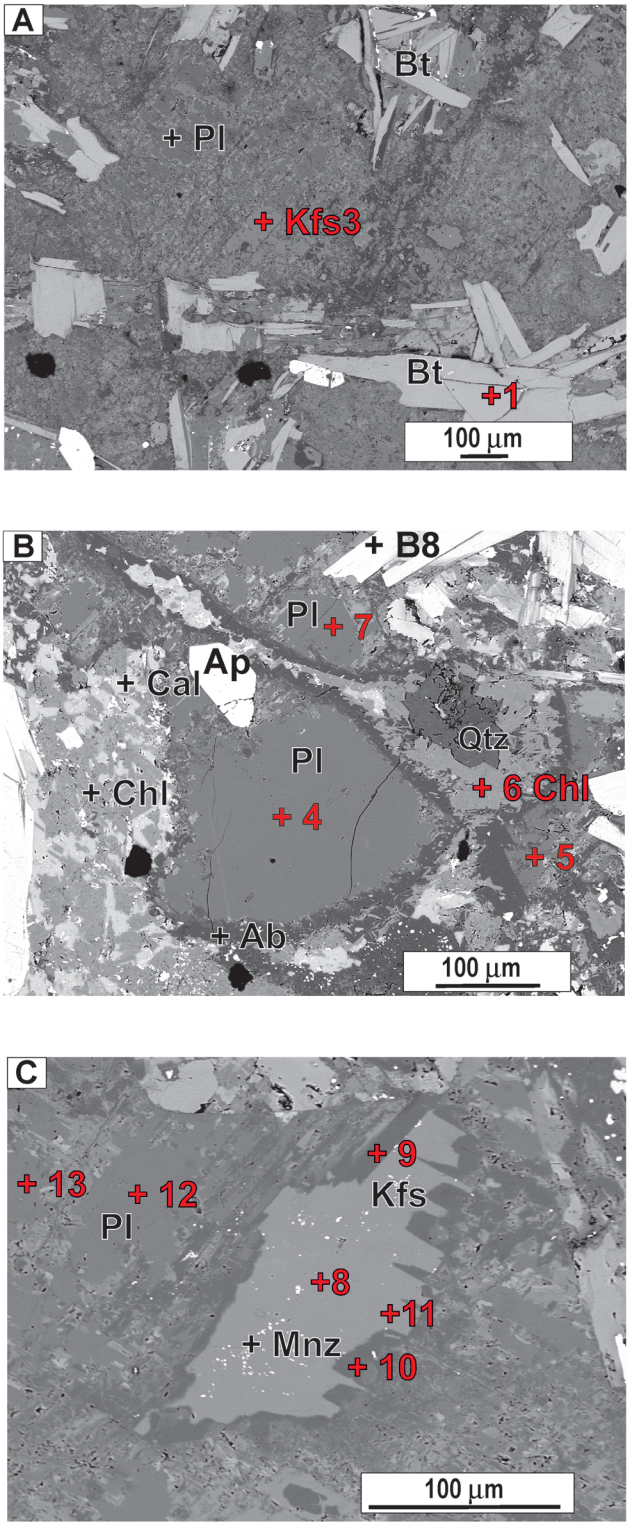

Fig. 9. Back-scattered electron (BSE) images of minerals in the studied gabbro-dioritoid (Zel-1c); the analyses numbers in figures correspond to those in Tables 1, 3. *Abbreviations*: Pl – plagioclase, Bt – biotite, Kfs – K-feldspar, Chl – chlorite, Ab – albite, Ap – apatite, Cal – calcite, Mnz – monazite.

Source and further petrogenesis

The isotopic composition (Sr–Nd–Pb) of the studied mafic rocks [$(^{87}Sr/^{86}Sr)_{360}$=0.7035–0.7048, $(^{143}Nd/^{144}Nd)_{360}$= 0.51224–0.51226 with εNd_{360}=+1.22 to +1.60] preclude a simple depleted mantle origin. Instead, mafic intrusions that have initial Nd isotope ratios close to the chondritic value (εNd=0) call for several genetic scenarios, including: (1) generation from primitive mantle, i.e., chondritic mantle with no previous melting or enrichment history; (2) partial melting of a mantle that underwent enrichment of a previously-depleted mantle source – including arcs and subcontinental lithospheric mantle (SCLM); (3) partial melting of relatively young and primitive, metabasic crust or (4) mixing of depleted-mantle-derived mafic melts with continental crustal material, either molten (i.e., granitic melt) or assimilated (AFC).

Mixing models based on Sr–Nd isotopic data were used to constrain any possible genesis of the NTM gabbro-dioritoids (Fig. 15). Input isotopic parameters for probable sources involved in the mixing model came from published works (Kohút et al. 1999, 2008; Poller et al. 2001; Kohút & Nabelek 2008) and are presented in Table 7. Since the Devonian gabbro (Kohút & Nabelek 2008) exhibits the most primitive isotopic (Sr–Nd) characteristics of the pre-Mesozoic basement igneous rocks of the CWC, it was chosen as a possible depleted-mantle-derived end-member. Based on of the isotopic compositions, Kohút & Nabelek (2008) postulated a vertically-zoned, lower crust consisting of old metaigneous (amphibolitic) and metasedimentary rocks as other plausible sources of the CWC Variscan granitic rocks. Therefore, typical representatives of both rock types were used in the mixing models as well (see Table 7, Fig. 15).

It is important to note that the results of mixing modelling indicate dominance of a depleted mantle-derived melt with at least ca. 50 % component that is akin to the composition of the Devonian gabbro in the NTM diorites. On the other hand, their crustal heritage could be represented by a ca. 30 % component having origin in the older amphibolitic rocks with an additional contribution of ca. 20 % from the common CWC metasedimentary rocks. Hence, the NTM dioritoids yield Nd model ages (t_{DM2st}) significantly older than their U–Pb crystallization ages. Indeed, the resulting dioritic initial Sr–Nd isotopic data would be only slightly less evolved than the average composition of the Devonian Bulk Silicate Earth (BSE; Fig. 15).

The unsystematic increase in Pb isotope ratios of the NTM diorites compared to common mantle reservoirs (e.g., the DM and MORB and/or the BSE and Lower crust, see Fig. 16) indicates either melting of an ancient EM-II reservoir, which could be generated by subduction of terrigenous sediment and/or mature continental crustal material into the mantle, followed by several hundred million years of mantle ageing, or upper crustal contamination of mantle-derived magma in the magmatic arc (Hart 1988). However, unproportionally increased $^{206}Pb/^{204}Pb$ compared to $^{207}Pb/^{204}Pb$ can call rather

Table 3: The chemical composition of the studied feldspars.

N. anal.	4	5	7	9	10	12	13	Kfs3	Kfs8	Kfs11
Fig.	Fig 8b	Fig 8b	Fig 8b	Fig 8c	Fig 8c	Fig 8c	Fig 8c	Fig. 8a	Fig. 8c	Fig. 8c
SiO_2	61.17	62.24	60.59	69.37	69.81	61.50	61.72	66.05	64.69	65.69
TiO_2	0.05	0.00	0.05	0.00	0.00	0.00	0.00	0.01	0.00	0.00
Al_2O_3	23.70	23.03	23.93	18.88	19.16	23.76	23.63	17.32	17.38	17.63
FeO^+	0.10	0.15	0.20	0.08	0.09	0.13	0.12	0.14	0.11	0.06
MnO	0.02	0.00	0.01	0.00	0.00	0.00	0.00	0.04	0.00	0.00
CaO	5.92	5.08	5.97	0.01	0.02	5.55	5.70	0.00	0.10	0.00
MgO	0.00	0.00	0.02	0.00	0.00	0.00	0.00	0.01	0.00	0.00
BaO	0.00	0.00	0.00	0.00	0.00	0.00	0.00	0.00	0.01	0.00
SrO	0.00	0.47	0.00	0.00	0.00	0.52	0.44	0.00	0.00	0.00
Na_2O	7.38	8.35	7.26	11.34	11.24	7.92	7.85	0.25	0.17	0.23
K_2O	0.23	0.22	0.22	0.09	0.07	0.19	0.19	16.67	16.31	16.38
Total	98.57	99.53	98.25	99.76	100.39	99.57	99.66	100.48	98.76	100.01
Formula based on 8 oxygens										
Si	2.75	2.78	2.73	3.03	3.03	2.75	2.76	3.05	3.04	3.04
Ti	0.00	0.00	0.00	0.00	0.00	0.00	0.00	0.00	0.00	0.00
Al	1.25	1.21	1.27	0.97	0.98	1.25	1.24	0.94	0.96	0.96
Fe^{3+}	0.00	0.00	0.01	0.00	0.00	0.00	0.00	0.00	0.00	0.00
Fe^{2+}	0.00	0.00	0.00	0.00	0.00	0.00	0.00	0.01	0.00	0.00
Mn	0.00	0.00	0.00	0.00	0.00	0.00	0.00	0.00	0.00	0.00
Mg	0.00	0.00	0.00	0.00	0.00	0.00	0.00	0.00	0.01	0.00
Ca	0.29	0.24	0.29	0.00	0.00	0.27	0.27	0.00	0.00	0.00
Na	0.64	0.72	0.63	0.96	0.94	0.69	0.68	0.02	0.02	0.02
K	0.01	0.01	0.01	0.00	0.00	0.01	0.01	0.98	0.98	0.97
SUM	4.95	4.98	4.95	4.97	4.96	4.97	4.97	5.00	5.00	5.00
Ab%	68.12	73.90	67.81	99.44	99.50	71.30	70.57	0.00	0.00	0.00
An%	30.48	24.83	30.85	0.06	0.10	27.60	28.31	0.02	0.02	0.02
Or%	1.40	1.27	1.34	0.50	0.40	1.10	1.13	0.98	0.98	0.98

FeO* is total Fe as FeO

for an upper crustal contamination and/or local fluid alteration of the analysed dioritoid.

Geodynamic scenario

Broska et al. (2022) proposed that a slab break-off in the subducting oceanic crust could have been a mechanism responsible for the origin of the dioritic rocks in the Vysoké Tatry Mts. Generally, we agree that during the continent–continent or arc–continent collisions, slab detachment (slab break-off model according Davies & von Blanckenburg 1995) is to be followed by the upwelling of a relatively hot asthenosphere, leading in many cases to magmatism in the lithospheric mantle and overlying continental crust, including generation of calc-alkaline basalts. However, similar enriched calc-alkaline basalts can also be generated directly in the continental arc environment as indicated by the data presented in the current paper.

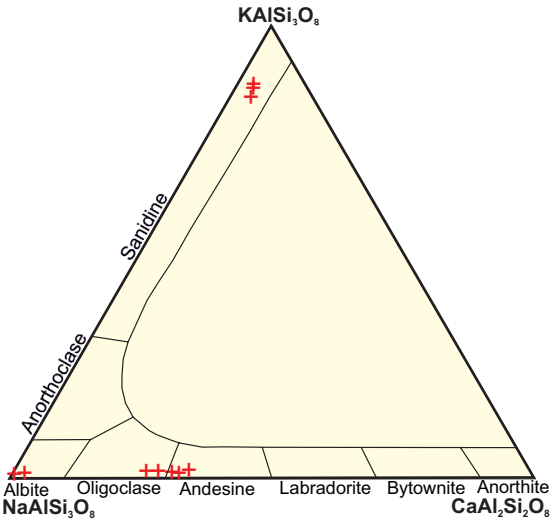

Fig. 10. Classification diagram of feldspars (from Deer et al. 1992).

Conclusions

- The magmatic ages for the Veľké Železné gabbro-dioritoids acquired from zircons (362.4±2.9 Ma) and apatites (358.4±2.8 Ma) by the LA-ICP-MS method indicate Famennian emplacement at ca. 360 Ma, followed by rapid magmatic crystallization and cooling of the studied gabbro-dioritoids.
- Isotopic signature with $(^{87}Sr/^{86}Sr)_{360}=0.7035–0.7044$, $\varepsilon Nd_{360}=+1.4$ to $+1.6$ and present-day $^{206}Pb/^{204}Pb=19.347$, $^{207}Pb/^{204}Pb=15.657$, $^{208}Pb/^{204}Pb=38.986$ reveals that the studied gabbro-dioritoids were formed from the mantle–

Table 4: Whole-rock chemical compositions of the studied gabbro-dioritoid rocks from the Veľké Železné area (Zel-1+2 this study, K-1 Koutek (1931) compared to the published NTM diorite data taken from Kohút & Recio (2002); Poller et al. (2005); Magna et al. (2010); Maraszewska et al. (2022).

Sample	Zel-1	Zel-2	K-1	UP-1116	UP-1116b	UP-1119	UP-1095	NT-487	NTM-25
SiO_2	49.59	51.25	47.64	59.35	59.40	59.26	59.09	54.84	57.50
TiO_2	1.35	1.34	1.27	0.89	0.87	0.94	0.86	1.03	1.19
Al_2O_3	13.80	14.10	12.82	15.71	15.53	16.02	15.23	14.78	16.93
Fe_2O_3	8.51	8.10	8.90	6.64	7.50	6.91	8.08	7.39	7.55
MnO	0.11	0.11	0.17	0.12	0.16	0.13	0.17	0.18	0.09
MgO	9.12	9.92	12.17	3.92	3.87	3.86	4.01	8.32	3.57
CaO	4.99	4.10	6.77	4.07	4.21	3.76	4.96	5.58	1.86
Na_2O	2.28	2.48	1.87	3.85	3.53	3.60	3.42	2.67	2.54
K_2O	2.69	2.75	2.49	2.97	2.68	3.31	2.26	2.63	5.43
P_2O_5	0.32	0.29	1.28	0.27	0.28	0.29	0.33	0.46	0.44
LOI	5.90	5.51	1.96	1.85	1.38	1.34	1.37	2.04	2.40
Total	98.66	99.95	97.34	99.64	99.41	99.42	99.78	99.92	99.50
mg#	67.98	70.81	71.59	53.91	50.55	52.53	49.58	69.04	48.37
A/NK	2.07	2.00	2.22	1.65	1.78	1.69	1.89	2.04	1.68
A/CNK	0.88	0.97	0.71	0.93	0.95	0.98	0.89	0.85	1.26
K_2O/Na_2O	1.18	1.11	1.33	0.77	0.76	0.92	0.66	0.99	2.14
Fe-number	0.46	0.42	0.41	0.60	0.64	0.62	0.65	0.44	0.66
MALI	−0.02	1.13	−2.41	2.75	2.00	3.15	0.72	−0.28	6.11
ASI	0.92	1.02	0.85	0.96	0.99	1.02	0.93	0.91	1.37
P	−105.44	−94.75	−128.20	−133.75	−132.08	−112.94	−150.82	−129.82	0.16
Q	85.13	97.19	70.63	93.61	108.71	97.65	110.54	95.93	99.66
V	272	248	–	102	120	19	147	110	147
Cr	233	198	–	59	97	64	143	416	-
Co	35	35.2	–	37	48	57	52	28	13.3
Ni	52.2	58	–	25	27	29	24	144	8.5
Cu	26.1	–	–	7	6	4	5	38	7.8
Zn	63	–	–	102	118	121	146	91	130
Ga	17	16.3	–	21	23	23	24	25	26.6
Rb	75.9	63.5	–	151	143	181	74	102	194.2
Sr	444	779.5	–	416	485	366	604	680	309.1
Y	27.8	20.1	–	23	28	22	30	20	19.6
Zr	129.9	111.1	–	181	178	207	152	150	203.1
Nb	10.9	7.7	–	10	9	11	7	15	13.8
Cs	12.4	9.6	–	11.3	11.7	11.5	12.1	12.3	12.4
Ba	1570	1394	–	623	628	737	551	650	1244
La	50.30	40.80	–	18.65	19.65	24.00	19.05	43.95	40.90
Ce	129.80	94.00	–	41.50	43.50	56.00	42.80	96.62	93.30
Pr	16.41	12.17	–	5.82	5.90	7.52	5.63	11.83	11.73
Nd	69.10	50.70	–	25.70	25.30	32.30	24.30	42.34	48.70
Sm	12.53	8.89	–	6.35	6.58	7.50	6.65	7.28	9.86
Eu	2.84	2.17	–	1.65	1.80	2.05	1.70	1.95	1.97
Gd	8.71	6.71	–	6.30	6.60	7.10	6.50	7.68	7.77
Tb	1.24	0.82	–	0.85	0.95	1.10	0.90	1.15	0.92
Dy	5.79	4.40	–	5.10	5.40	5.90	5.30	5.56	4.42
Ho	1.20	0.75	–	0.92	1.00	1.10	0.95	1.07	0.69
Er	3.14	2.02	–	2.35	2.50	2.82	2.40	2.51	1.71
Tm	0.47	0.29	–	0.31	0.34	0.37	0.33	0.35	0.22
Yb	2.58	1.77	–	1.95	2.08	2.21	1.98	1.95	1.31
Lu	0.43	0.27	–	0.26	0.29	0.35	0.28	0.34	0.19
Hf	4.3	3.8	–	5.3	5.1	5.6	5.2	4.7	5.1
Ta	0.8	0.5	–	0.4	0.4	0.4	0.4	0.5	0.5
Pb	4.7	5.3	–	11	8	8	9	6	5.9
Th	10.5	13.6	–	6.8	6.4	6.3	6.2	10.2	15.5
U	4.3	4.3	–	2.3	2.2	2.1	2.1	3.5	1.9
Eu/Eu*	0.83	0.86	–	0.80	0.84	0.86	0.79	0.80	0.69
La_N/Yb_N	13.14	15.54	–	6.45	6.37	7.32	6.49	15.20	21.05
La_N/Sm_N	2.53	2.89	–	1.85	1.88	2.01	1.80	3.80	2.61
Eu_N/Yb_N	3.13	3.49	–	2.41	2.46	2.64	2.44	2.84	4.28
Sum REE	304.54	225.76	–	117.71	121.89	150.32	118.77	224.58	223.69

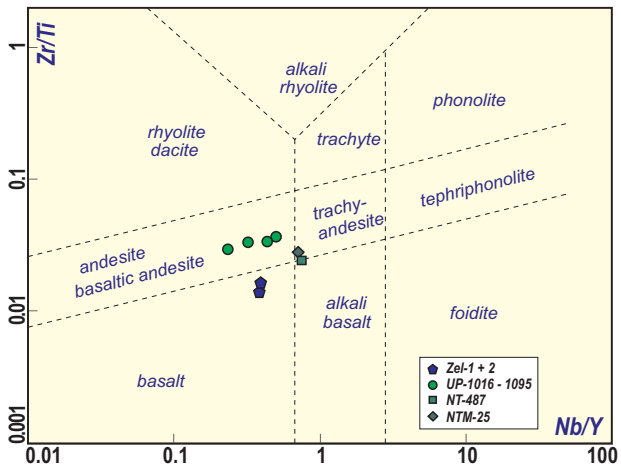

Fig. 11. The Zr/Ti vs. Nb/Y classification diagram of basaltic rocks (Pearce 1996).

influenced lower crustal and/or sub-continental lithospheric mantle sources, and/or an ancient Enriched mantle-II reservoir was melted there and later modified by a partial fluid alteration.

- The Sr–Nd isotope mixing models, using the characteristics of possible local end members, imply that the magma derived from the older gabbroic mantle (50 %) could have mixed with melt from the lower crustal amphibolites (30 %) and metasediments (20 %).
- The presented data suggest the origin of the Veľké Železné gabbro-dioritoids in the continental arc geodynamic setting; however, the slab break-off model cannot be ruled out as a possible mechanism of their genesis.

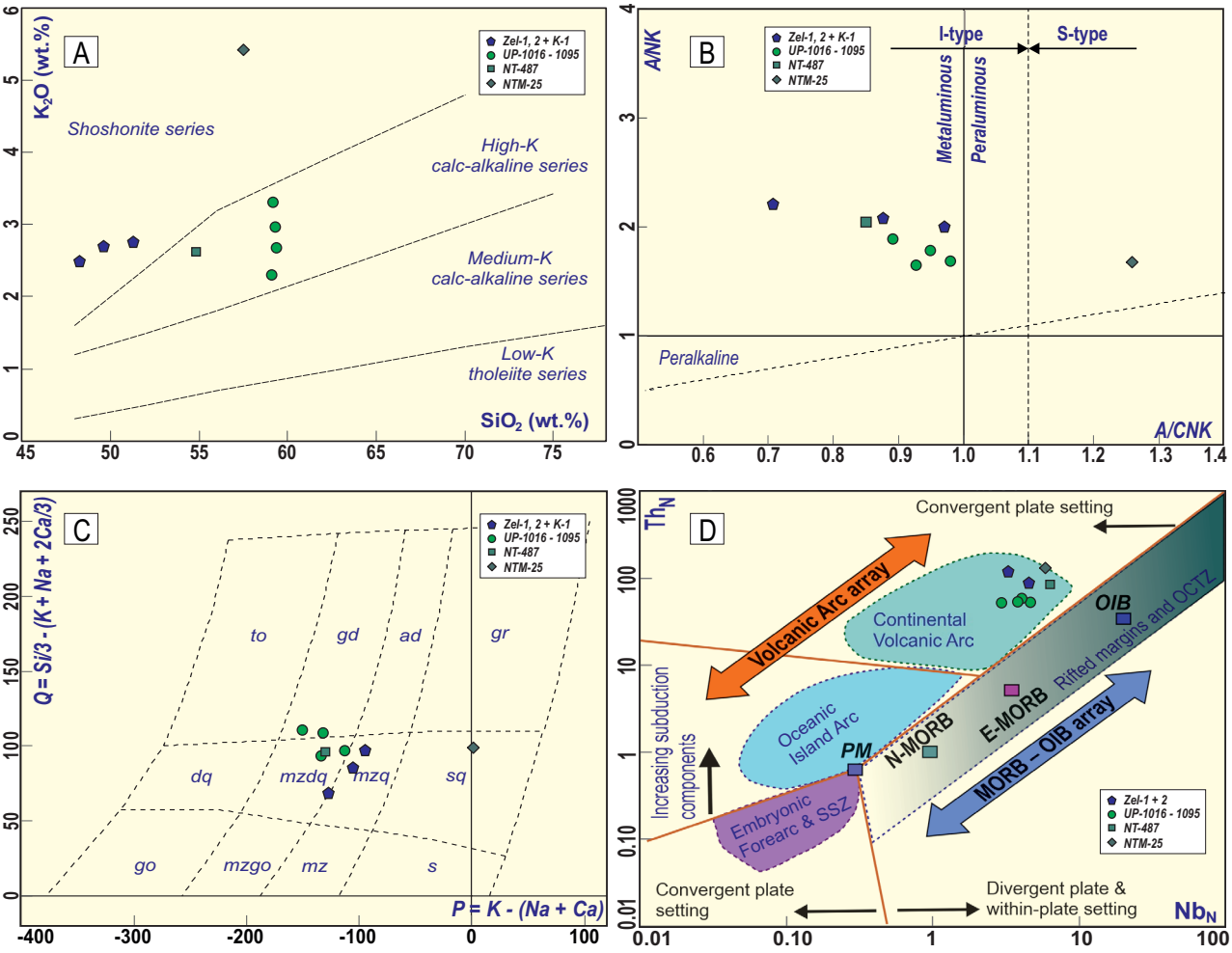

Fig. 12. A — K_2O vs. SiO_2 plot for the gabbro-dioritoids of the NTM (Peccerillo & Taylor 1976); **B** — A/NK vs. A/CNK plot according to Shand (1943), I-type vs. S-type granite boundary after Chappell & White (1992); **C** — P–Q diagram (Debon & Le Fort 1983) in millications, P=K–(Na+Ca) and Q=Si/3–(K+Na+2×Ca/3) where P represents the cation proportion of K-feldspar to plagioclase, and Q the quartz content. *Abbreviations*: mzdq – quartz monzodiorite, mzq – quartz monzonite, gd – granodiorite; **D** — diagram of Saccani (2015) based on NMORB-normalized $Th_{[N]}$ vs. $Nb_{[N]}$ values (Sun & McDonough 1989) for discrimination of geotectonic setting of the basaltic rocks. *Abbreviation*: OCTZ – Ocean–Continent Transition Zones.

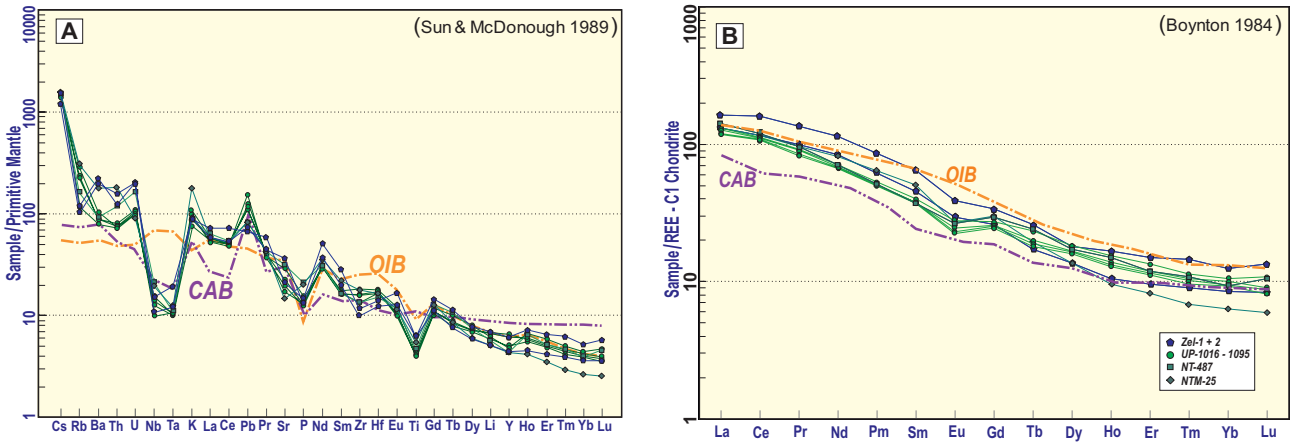

Fig. 13. A — Primitive mantle-normalized (Sun & McDonough 1989) multi-element plots of the Veľké Železné gabbro-dioritoids and **B** — C1 chondrite-normalized (Boynton 1984). *Abbreviations*: CAB – continental arc basalt (Li et al. 2017); OIB – ocean island basalt (Sun & McDonough 1989).

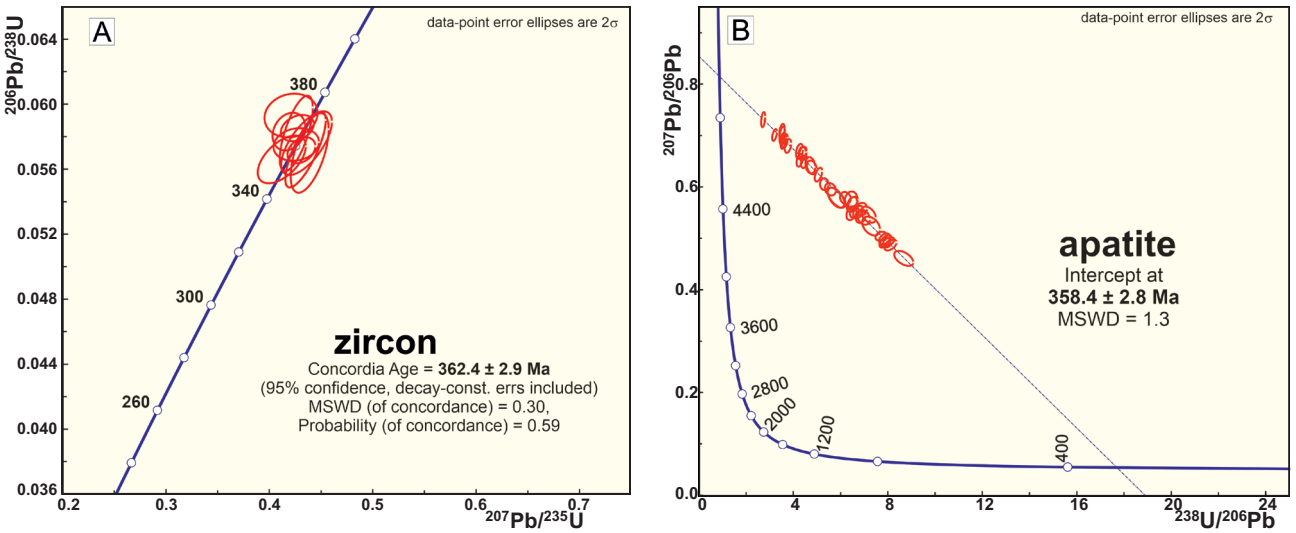

Fig. 14. LA-ICP-MS U–Pb ages for the Veľké Železné gabbro-dioritoid sample Zel-1: **A** — concordia diagram for analysed zircons; **B** — Tera-Wasserburg plot for analysed apatites.

Table 5: Radiogenic Sr and Nd isotope data and calculated parameters of the investigated gabbro-dioritoid samples and the published data from NTM dioritic rocks. Values of Rb, Sr, Sm and Nd are in ppm; T_{DM} and $T_{DM(2st)}$ in Ga. NT-487 data taken from Magna et al. (2010), UP-1116 and UP-1119 taken from Poller et al. (2005).

Sample	Rb	Sr	$^{87}Rb/^{86}Sr$	$^{87}Sr/^{86}Sr$	2σ	$^{87}Sr/^{86}Sr_{(i)}$	Sm	Nd	$^{147}Sm/^{144}Nd$	$^{143}Nd/^{144}Nd$	2σ	$^{143}Nd/^{144}Nd_{(i)}$	$eNd_{(i)}$	t_{DM}	$t_{DM(2st)}$
Zel-1	75.9	444	0.494516	0.706050	±8	0.703516	12.22	66.51	0.111035	0.512518	±9	0.512256	1.60	0.89	0.94
Zel-2	63.5	779.5	0.235645	0.705561	±10	0.704353	22.82	124.99	0.110350	0.512506	±11	0.512246	1.40	0.90	0.96
NT-487	102	680	0.433968	0.707096	±12	0.704872	7.28	42.34	0.103947	0.512482	±10	0.512237	1.22	0.89	0.97
UP-1116	151	416	1.050440	0.709937	±10	0.704553	7.83	35.37	0.133834	0.512566	±20	0.512251	1.49	1.05	0.95
UP-1119	181	366	1.431413	0.711798	±16	0.704462	4.36	28.33	0.093040	0.512465	±24	0.512246	1.39	0.83	0.96

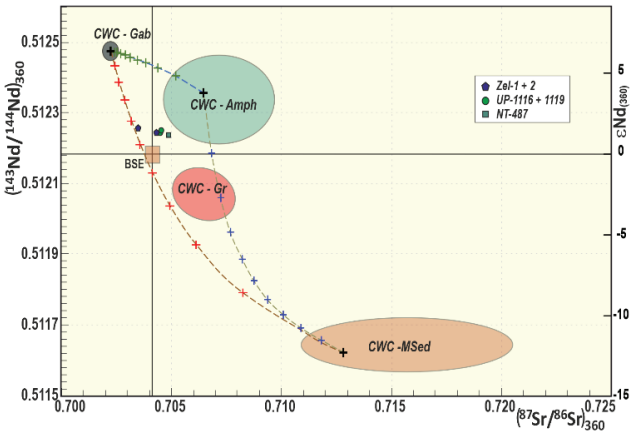

Fig. 15. Initial Nd and Sr isotopic compositions for gabbro-dioritoids of the Nízke Tatry Mts. compared with those from the Western Carpathians crystalline basement. *Abbreviations*: BSE – Bulk Silicate Earth, CWC-Amph – amphibolites from the Western Carpathians, CWC-Gab – Devonian gabbros of the CWC, CWC-Gr – granitic rocks of the CWC, CWC-MSed – meta-sediments of the CWC. Data taken from Kohút et al. (1999, 2008), Poller et al. (2001, 2005), and unpublished data Kohút & Poller. Dashed lines refer to possible mixing hyperbolas (Janoušek et al. 2016).

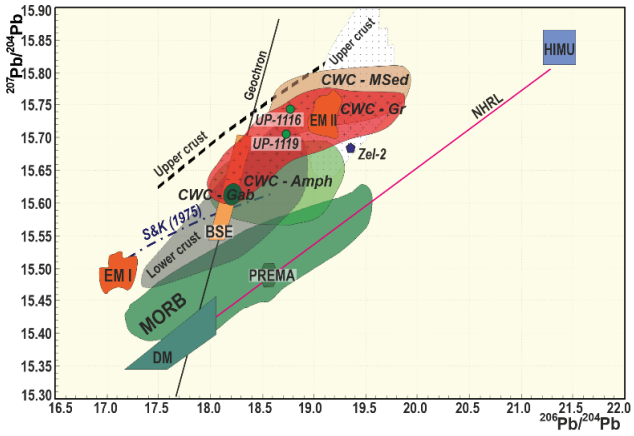

Fig. 16. $^{207}Pb/^{204}Pb$ vs. $^{206}Pb/^{204}Pb$ correlation plot with indication of reference fields according Doe & Zartman (1979) and Zindler & Hart (1986). Plotted are also fields of the Western Carpathians basement rocks after Poller et al. (2001, 2005) and Kohút et al. (2008). *Abbreviations*: BSE, CWC-Amph, CWC-Gab, CWC-Gr, CWC-MSed as in Fig. 15; DM – Depleted Mantle, EM-I – Enriched Mantle I, EM-II – Enriched Mantle II, HIMU – High-μ (high $^{238}U/^{204}Pb$) mantle reservoir, MORB – Mid-Ocean Ridge Basalts, NHRL – Northern Hemisphere Reference Line, PREMA – PRevalent MAntle, S&K (1975) – Stacey & Kramers (1975) reference line.

Table 6: Lead isotope data from the Veľké Železné Valley gabbro-dioritoid sample Zel-2 and the published data from NTM dioritic rocks. UP-1116 and UP-1119 data taken from Poller et al. (2005).

Sample	$^{206}Pb/^{204}Pb$	± 2σ	$^{207}Pb/^{204}Pb$	± 2σ	$^{208}Pb/^{204}Pb$	± 2σ
Zel-2	19.3469	0.0090	15.6570	0.0093	38.9860	0.0283
UP-1116	18.7721	0.0005	15.7431	0.0005	38.6886	0.0005
UP-1119	18.7216	0.0005	15.7001	0.0005	38.5276	0.0005

Table 7: Input parameters for individual sources in the mixing models (taken from Kohút & Nabelek 2008).

	Sr	$(^{87}Sr/^{86}Sr)_{360}$	Nd	$(^{143}Nd/^{144}Nd)_{360}$
Gabbro	638	0.702321	65.68	0.512474
Amphibolite	165	0.706501	10.80	0.512355
Metapelite	93	0.712883	29.70	0.511623

Acknowledgments: This work was supported by the Slovak Research and Development Agency under the Contract no. APVV-22-0092, APVV-19-0065 and VEGA 1/0563/22. Constructive reviews and valuable comments by Vojtěch Janoušek and Martin Ondrejka helped to improve the manuscript; Igor Broska is thanked for editorial handling.

References

Arth J.G. & Hanson G.N. 1972: Quartz diorites derived by partial melting of eclogite or amphibolite at mantle depths. *Contributions to Mineralogy and Petrology* 37, 161–174. https://doi.org/10.1007/BF00371074

Arth J.G., Barker F., Peterman Z.E. & Friedman I. 1978: Geochemistry of the gabbro–diorite–tonalite–trondhjemite suite of southwest Finland and its implications for the origin of tonalitic and trondhjemitic magmas. *Journal of Petrology* 19, 289–316. https://doi.org/10.1093/petrology/19.2.289

Barbarin B. 2005: Mafic magmatic enclaves and mafic rocks associated with some granitoids of the central Sierra Nevada Batholith, California: nature, origin, and relations with the hosts. *Lithos* 80, 155–177. https://doi.org/10.1016/j.lithos.2004.05.010

Bea F., Montero P. & Molina F. 1999: Mafic precursors, peraluminous granitoids, and late lamprophyres in the Ávila Batholith: a model for the generation of Variscan batholiths in Iberia. *The Journal of Geology* 107, 399–419. https://doi.org/10.1086/314356

Biely A. (Ed.), Beňuška P., Bezák V., Bujnovský A., Halouzka R., Ivanička J., Kohút M., Klinec A., Lukáčik E., Maglay J., Miko O., Pulec M., Putiš M. & Vozár J. 1992: Geological map of the Nízke Tatry Mountains in a scale 1:50,000. *Dionýz Štúr Institute of Geology Publishing House*, Bratislava.

Black L.P., Kamo S.L., Williams I.S., Mundil R., Davis D.W., Korsch R.J. & Foudoulis C. 2003: The application of SHRIMP to Phanerozoic geochronology; a critical appraisal of four zircon standards. *Chemical Geology* 200, 171–188. https://doi.org/10.1016/S0009-2541(03)00166-9

Bowes D.R. & McArthur A.C. 1976: Nature and genesis of the appinite suite. *Krystalinikum* 12, 31–46.

Boynton W.V. 1984: Cosmochemistry of the rare earth elements: meteorite studies. In: Henderson P. (Ed.): Rare Earth Element Geochemistry. Developments in Geochemistry, Vol. 2. *Elsevier*, Amsterdam, 63–114. https://doi.org/10.1016/B978-0-444-42148-7.50008-3

Broska I. & Petrík I. 1993: Magmatic enclaves in granitic rocks of the Western Carpathians. *Mineralia Slovaca* 25, 104–108 (in Slovak with English summary).

Broska I., Petrík I., Be'eri-Shlevin Y., Majka J. & Bezák V. 2013: Devonian/Mississippian I-type granitoids in the Western Carpathians: a subduction-related hybrid magmatism. *Lithos* 162, 27–36. https://doi.org/10.1016/j.lithos.2012.12.014

Broska I., Janák M., Svojtka M., Yi K., Konečný P., Kubiš M., Kurylo S., Hrdlička M. & Maraszewska M. 2022: Variscan granitic magmatism in the Western Carpathians with linkage to slab break-off. *Lithos* 412–413, 106589. https://doi.org/10.1016/j.lithos.2021.106589

Cabanis B. & Lecolle M. 1989: Le diagramme La/10–Y/15–Nb/8: un outil pour la discrimination des séries volcaniques et la mise en évidence des processus de mélange et/ou de contamination crustale. *Comptes Rendus de l'Académie des Sciences*. Série 2, Mécanique, Physique, Chimie, Sciences de l'Univers, Sciences de la Terre 309, 2023–2029.

Chappell B.W. & White A.J.R. 1992: I-and S-type granites in the Lachlan Fold Belt. *Transactions of the Royal Society of Edinburgh, Earth Sciences* 83, 1–26. https://doi.org/10.1017/S0263593300007720

Chew D.M., Petrus J.A. & Kamber B.S. 2014: U–Pb LA–ICPMS dating using accessory mineral standards with variable common Pb. *Chemical Geology* 363, 1850150199. https://doi.org/10.1016/j.chemgeo.2013.11.006

Cochrane R., Spikings R.A., Chew D., Wotzlaw J.F., Chiaradia M., Tyrrell S., Schaltegger U. & Van der Lelij R. 2014: High temperature (>350 °C) thermochronology and mechanisms of Pb loss in apatite. *Geochimica et Cosmochimica Acta* 127, 39–56. https://doi.org/10.1016/j.gca.2013.11.028

Danišík M., Kadlec J., Glotzbach C., Weisheit A., Dunkl I., Kohút M., Evans N.J., Orvošová M. & McDonald B.J. 2011: Tracing metamorphism, exhumation and topographic evolution in orogenic belts by multiple thermochronology: a case study from the Nízke Tatry Mts., Western Carpathians. *Swiss Journal of Geosciences* 104, 285–298. https://doi.org/10.1007/s00015-011-0060-6

Davies J.H. & von Blanckenburg F. 1995: Slab breakoff: a model of lithosphere detachment and its test in the magmatism and deformation of collisional orogens. *Earth and Planetary Science Letters* 129, 85–102. https://doi.org/10.1016/0012-821X(94)00237-S

Debon F. & Le Fort P. 1983: A chemical-mineralogical classification of common plutonic rocks and associations. *Transactions of the Royal Society of Edinburgh, Earth Sciences* 73, 135–149. https://doi.org/10.1017/S0263593300010117

Deer W.A., Howie A. & Zussman J. 1992: An Introduction to the Rock-Forming Minerals. 2nd ed., *Pearson,* Harlow, 1–696.

Didier J. & Barbarin B. 1991: The different types of enclaves in granites – Nomenclature. In: Didier J. & Barbarin B. (eds.): Enclaves and granite petrology. *Developments in Petrology* 13, *Elsevier*, Amsterdam,19–23.

Doe B.R. & Zartman R.E. 1979: Plumbotectonics, I. The Phanerozoic. In: Barnes H.L. (Ed.): Geochemistry of Hydrothermal Ore Deposits. 2nd ed., Chapter 2, *Wiley Intersci. Publ. House*, New York, 22–70.

Gawęda A., Doniecki T., Burda J. & Kohút M. 2005: The petrogenesis of quartz-diorites from the Tatra Mountains (Central Western Carpathians): an example of magma hybridisation. *Neues Jahrbuch für Mineralogie – Abhandlungen* 181, 95–109. http://doi.org/10.1127/0077-7757/2005/0181-0005

Gawęda A. Szopa K. & Chew D. 2014: LA-ICP-MS U–Pb dating and REE patterns of apatite from the Tatra Mountains, Poland as a monitor of the regional tectonomagmatic activity. *Geochronometria* 41, 306–314. https://doi.org/10.2478/s13386-013-0171-0

Hart S.R. 1988: Heterogeneous mantle domains: signatures, genesis and mixing chronologies. *Earth and Planetary Science Letters* 90, 273–296. https://doi.org/10.1016/0012-821X(88)90131-8

Hawthorne C.F., Oberti R., Harlow G.E., MareschV.W., Martin F.R., Schumacher C.J. & Welch D.M. 2012: Nomenclature of the amphibole supergroup. *American Mineralogist* 97, 2031–2048. https://doi.org/10.2138/am.2012.4276

Hollocher K., Robinson P., Walsh E. & Roberts D. 2012: Geochemistry of amphibolite-facies volcanics and gabbros of the Støren Nappe in extensions west and southwest of Trondheim, Western Gneiss Region, Norway: a key to correlations and paleotectonic settings. *American Journal of Science* 312, 357–416. https://doi.org/10.2475/04.2012.01

Horwitz E.P., Chiarizia R. & Dietz M.L. 1992: A novel strontium-selective extraction chromatographic resin. *Solvent Extraction and Ion Exchange* 10, 313–36.

Hovorka D. 1967: Porphyrites and lamprophyres of the Tatric–Veporic crystalline basement. *Sborník geologických vied, Západné Karpaty, rad ZK* 8, 51–78 (in Slovak with English summary).

Janoušek V., Moyen J.F., Martin H., Erban V. & Farrow C. 2016: Geochemical Modelling of Igneous Processes: Principles and Recipes in R Language. Bringing the Power of R to a Geochemical Community. *Springer-Verlag*, Berlin, Heidelberg. https://doi.org/10.1007/978-3-662-46792-3

Janoušek V., Bonin B., Collins W.J., Farina F. & Bowden P. 2020: Post-Archean granitic rocks: contrasting petrogenetic processes and tectonic environments. In: Janoušek V., Bonin B., Collins W.J., Farina F. & Bowden P. (Eds): Post-Archean Granitic Rocks: Petrogenetic Processes and Tectonic Environments. *Geological Society, London*, *Special Publications* 491, 1–8. https://doi.org/10.1144/SP491-2019-197

Jung S., Hoernes S. & Mezger K. 2002: Synorogenic melting of mafic lower crust: constraints from geochronology, petrology and Sr, Nd, Pb and O isotope geochemistry of quartz diorites (Damara Orogen, Namibia). *Contributions to Mineralogy and Petrology* 143, 551–566. https://doi.org/10.1007/s00410-002-0366-5

Kohút M. 1998: Some geochemical remarks to genesis of the granitic rocks from the Nízke Tatry Mts. *Mineralia Slovaca* 30, 83–84 (in Slovak).

Kohút M. & Larionov A.N. 2021: From subduction to collision: genesis of the Variscan granitic rocks from the Tatric Superunit (Western Carpathians, Slovakia). *Geologica Carpathica* 72, 96–113. https://doi.org/10.31577/GeolCarp.72.2.2

Kohút M. & Nabelek P.I. 2008: Geochemical and isotopic (Sr, Nd and O) constraints on sources for Variscan granites in the Western Carpathians – implications for crustal structure and tectonics. *Journal of Geosciences* 53, 307–322. https://doi.org/10.3190/jgeosci.033

Kohút M. & Recio C. 2002: Sulphur isotopes of selected Hercynian granitic and surrounding rocks from the Western Carpathians (Slovakia). *Geologica Carpathica* 53, 3–13.

Kohút M., Kotov A.B., Salnikova E.B. & Kovach V.P. 1999: Sr and Nd isotope geochemistry of Hercynian granitic rocks from the Western Carpathians – implications for granite genesis and crustal evolution. *Geologica Carpathica* 50, 477–487.

Kohút M., Poller U., Gurk C. & Todt W. 2008: Geochemistry and U–Pb detrital zircon ages of metasedimentary rocks of the Lower Unit, Western Tatra Mountains (Slovakia). *Acta Geologica Polonica* 58, 371–384.

Kohút M., Uher P., Putiš M., Ondrejka M., Sergeev S., Larionov A. & Paderin I. 2009: SHRIMP U–Th–Pb zircon dating of the granitoid massifs in the Malé Karpaty Mountains (Western Carpathians): evidence of Meso-Hercynian successive S-to I-type

granitic magmatism. *Geologica Carpathica* 60(5), 345–350. https://doi.org/10.2478/v10096-009-0026-z

Koutek J. 1931: Géologie du versant nord-ouest de la base Tatra. *Sborník Státního Geologického Ústavu (Bull. State Geol. Inst.)* 9, 289–302.

Kriváňová K., Vojtko R., Droppa D.M. & Gerátová S. 2023: Deformation record and revised tectonic evolution of the Nízke Tatry Mts. in the Tatric–Veporic junction area: Insights from structural analysis. *Geologica Carpathica* 74, 197–210. https://doi.org/10.31577/GeolCarp.2023.15

Li Y., Zhang Q., Wang J., Liu X., Chen W. 2017: Global active continental margin arc basalt (CAB) characteristics: compared with island arc basalt (IAB) and back – arc basin basalt (BAB). *Chinese Journal of Geology* 52, 693–713 (in Chinese with English abstract). https://doi.org.10.12017/dzkx.2017.044

Lukáčik E. 1981: Petrology of granite-granodiorites of the Prašivá type in the western part of the Nízke Tatry Mts. pluton. *Západné Karpaty* 8, 121–142.

Magna T., Janoušek V., Kohút M., Oberli F. & Wiechert U. 2010: Fingerprinting sources of orogenic plutonic rocks from Variscan belt with lithium isotopes and possible link to subduction-related origin of some A-type granites. *Chemical Geology* 274, 94–107. https://doi.org/10.1016/j.chemgeo.2010.03.020

Maraszewska M., Broska I., Kohút M., Yi K., Konečný P. & Kurylo S. 2022: The Ďumbier–Prašivá high K calc-alkaline granite suite (Low Tatra Mts., Western Carpathians): insights into their evolution from geochemistry and geochronology. *Geologica Carpathica* 73, 273–291. https://doi.org/10.31577/GeolCarp.73.4.1

McDowell F.W., McIntosh W.C. & Farley K.A. 2005: A precise ^{40}Ar–^{39}Ar reference age for the Durango apatite (U–Th)/He and fission-track dating standard. *Chemical Geology* 214, 249–263. https://doi.org/10.1016/j.chemgeo.2004.10.002

Meschede M. 1986: A method of discrimination between different types of mid-ocean ridge basalts and continental tholeiites with the Nb–Zr–Y diagram. *Chemical Geology* 56, 207–218. https://doi.org/10.1016/0009-2541(86)90004-5

Paton C., Hellstrom J., Paul B., Woodhead J., & Hergt J. 2011: Iolite: Freeware for the visualisation and processing of mass spectrometric data. *Journal of Analytical Atomic Spectrometry* 26, 2508–2518. https://doi.org/10.1039/C1JA10172B

Pearce J.A. 1996: A user's guide to basalt discrimination diagrams. In: Wyman D.A. (Ed.): Trace Element Geochemistry of Volcanic Rocks: Applications for Massive Sulphide Exploration. *Geological Association of Canada, Short Course Notes* 12, 79–113.

Pearce J.A. & Cann J.R. 1973: Tectonic setting of basic volcanic rocks determined using trace element analyses. *Earth Planetary Science Letters* 19, 290–300. https://doi.org/10.1016/0012-821X(73)90129-5

Pearce J.A., Alabaster T., Shelton A.W. & Searle M.P. 1981: The Oman ophiolite as a Cretaceous arc-basin complex: evidence and implications. *Philosophical Transactions of the Royal Society of London, Series A, Mathematical and Physical Sciences* 300, 299–317. https://doi.org/10.1098/rsta.1981.0066

Petrus J.A. & Kamber B.S. 2012: VizualAge: A novel approach to laser ablation ICP-MS U–Pb geochronology data reduction. *Geostandards and Geoanalytical Research* 36, 247–270. https://doi.org/10.1111/j.1751-908X.2012.00158.x

Peccerillo A. & Taylor S.R. 1976: Geochemistry of Eocene calc-alkaline volcanic rocks from the Kastamonu area, Northern Turkey. *Contribution to Mineralogy and Petrology* 58, 63–81. https://doi.org/10.1007/BF00384745

Pitcher W.S. 1997: The mingling and mixing of granite with basalt: a third term in a multiple hypothesis. In: The Nature and Origin of Granite. *Springer*, Dordrecht, 144–167. https://doi.org/10.1007/978-94-011-5832-9_9

Poller U. & Todt W. 2000: U–Pb single zircon data of granitoids from the High Tatra Mountains (Slovakia): implications for the geodynamic evolution. *Transactions of the Royal Society of Edinburgh*, *Earth Sciences* 91, 235–243. https://doi.org/10.1017/S0263593300007409

Poller U., Todt W., Kohút M. & Janák M. 2001: Nd, Sr, Pb isotope study of the Western Carpathians: implications for Palaeozoic evolution. *Schweizerische mineralogische und petrographische Mitteilungen* 81, 159–174. http://doi.org/10.5169/seals-61685

Poller U., Kohút M., Gaab A.S. & Todt W. 2005: Pb, Sr and Nd isotope study of two co-existing magmas in the Nízke Tatry Mountains, Western Carpathians (Slovakia). *Mineralogy and Petrology* 84, 215–231. https://doi.org/10.1007/s00710-005-0080-x

Rieder M., Cavazzini G., D'yakonov Y.S., Frank-Kamenetskii V.A., Gottardi G., Guggenheim S., Koval P.V., Müller G., Neiva A.M.R., Radoslovich E.W., Robert J.L., Sassi F.P., Takeda H., Weiss Z. & Wones D.R. 1998: Nomenclature of micas. *Canadian Mineral*ogist 36, 905–912. https://doi.org/10.1346/CCMN.1998.0460513

Saccani E. 2015: A new method of discriminating different types of post-Archean ophiolitic basalts and their tectonic significance using Th–Nb and Ce–Dy–Yb systematics. *Geoscience Frontiers* 6, 481–501. https://doi.org/10.1016/j.gsf.2014.03.006

Schoene B., & Bowring S.A. 2006: U–Pb systematics of the McClure Mountain syenite: thermochronological constraints on the age of the ^{40}Ar/^{39}Ar standard MMhb. *Contributions to Mineralogy and Petrology* 151, 615–630. https://doi.org/10.1007/s00410-006-0077-4

Shand S.J. 1943: Eruptive Rocks. 2nd ed. *John Wiley & Sons*, New York, 1–444.

Spišiak J., Mikuš T., Chew D., Vetráková L., Siman P. & Ferenc Š. 2017: Dioritic rocks from the Železné Valley (Nízke Tatry Mts.): petrology and geochemistry. In: Petros 2017 Conference Abstract book, 29–32 (in Slovak).

Stacey J.T. & Kramers I. 1975: Approximation of terrestrial lead isotope evolution by a two-stage model. *Earth and Planetary Science Letters* 26, 207–221. https://doi.org/10.1016/0012-821X(75)90088-6

Sun S.S. & McDonough W.F. 1989: Chemical and isotopic systematics of oceanic basalts: implications for mantle composition and processes. In: Saunders A.D. & Norry M.J. (eds.): Magmatism in the Ocean Basins. *Geological Society, London, Special Publications* 42, 313–345. https://doi.org/10.1144/GSL.SP.1989.042.01.19

Tanaka T., Togashi S., Kamiok H., Amakawa H., Kagam H., Hamamoto T., Yuhara M., Orihashi Y., Yoneda S., Shimizu H., Kunimaru T., Takahashi K., Yanagi T., Nakano T., Fujimaki H., Shinjo R., Asahara Y., Tanimizu M. & Dragusanu C. 2000: JNdi-1: A neodymium isotopic reference in consistency with La Jolla neodymium. *Chemical Geology* 168, 279–281. https://doi.org/10.1016/S0009-2541(00)00198-4

Thomson S.N., Gehrels G.E., Ruiz J. & Buchwaldt R. 2012: Routine low-damage apatite U–Pb dating using laser ablation-multi-collector-ICPMS. *Geochemistry, Geophysics, Geosystems* 13. https://doi.org/10.1029/2011GC003928

Todt W., Cliff R.A., Hanser A. & Hofmann A.W. 1993: Re-calibration of NBS lead standards using ^{202}Pb+^{205}Pb double spike. *Terra Abstract* 5, 396.

Uher P., Kohút M. & Putiš M. 2011: Hercynian dioritic rocks of the Western Carpathians: tracers of crustal–mantle interactions. *Travaux Géophysiques* 40, 86.

Uher P., Broska I., Vojtko P. & Kohút M. 2012: Zircon from the Hercynian dioritic rocks of the Western Carpathians: correlation of internal zonality to mineralogical and geochemical data. *Mineralia Slovaca, Geovestník* 44, 6–7 (in Slovak).

Wang X.C., Wilde S.A., Xu B. & Pang C.J. 2016: Origin of arc-like continental basalts: Implications for deep-Earth fluid cycling and tectonic discrimination. *Lithos* 261, 5–45. https://doi.org/10.1016/j.lithos.2015.12.014

White W.M. 2013: Geochemistry. *John Wiley and Sons*, New Jersey, 1–660.

Wiedenbeck M., Alle P., Corfu F.Y., Griffin W.L., Meier M., Oberli F.V., von Quadt A., Roddick J.C. & Spiegel W. 1995: Three natural zircon standards for U–Th–Pb, Lu–Hf, trace element and REE analyses. *Geostandards Newsletter* 19, 1–23. https://doi.org/10.1111/j.1751-908X.1995.tb00147.x

Wood D.A. 1980: The application of a Th–Hf–Ta diagram to problems of tectonomagmatic classification and to establishing the nature of crustal contamination of basaltic lavas of the British Tertiary volcanic province. *Earth Planetary Science Letters* 50, 11–30. https://doi.org/10.1016/0012-821X(80)90116-8

Zindler A. & Hart S. 1986: Chemical geodynamics. *Annual Review of Earth and Planetary Sciences* 14, 493–571. https://doi.org/10.1146/annurev.ea.14.050186.002425

Electronic supplementary material is available online:
Supplementary Tables S1 and S2 at http://geologicacarpathica.com/data/files/supplements/GC-75-1-Spisiak_TablesS1-S2.xlsx